Acknowledgements

Em primeiro lugar, quero agradecer à Doutora Margarida Duarte, orientadora deste estágio, por me ter acolhido de forma tão generosa no seu projeto e por me ter acompanhado ao longo deste ano. Obrigada por tudo aquilo que me ensinou, por toda a paciência e compreensão que teve comigo e por ter estado sempre tão presente. Foi muito importante para mim o seu apoio. Obrigada!

Agradeço à Doutora Ana Tomás, co-orientadora deste estágio, por me ter permitido trabalhar no seu laboratório. Agradeço também, por todas as ideias disponibilizadas para a evolução deste trabalho e pela disponibilidade que sempre demonstrou. Obrigada!

Agradeço de forma especial às minhas colegas de laboratório, Helena, Tânia, Sandra, Gina, Márcia e Matilde. Obrigada por estarem sempre dispostas a ajudar, pelo apoio que me deram sempre que precisei e por me terem feito sentir em “casa” desde o primeiro momento no laboratório. Obrigada meninas!

Agradeço também aos meus amigos pela paciência e compreensão que sempre têm comigo. Tenho de agradecer de forma especial aqueles que me “aturaram” intensivamente ao longo deste ano, foi muito bom viver esta experiência ao vosso lado! Vou sentir muito a vossa falta, falta do espírito de interajuda que conseguimos criar entre nós. Obrigada, é bom perceber que ainda existem pessoas como vocês. Continuarão comigo. Para Sempre.

Agradeço à minha família pela paciência que sempre têm comigo nestas fases mais complicadas. Obrigada pelo vosso constante apoio. Gosto muito de vocês.

Por último, agradeço aos meus pais que me apoiaram sempre, que aturaram todas as minhas frustrações, todos os meus momentos de desânimo, mas que também compartilharam as minhas pequenas, mas importantes, conquistas. Obrigada por tudo. Adoro-vos.

Abstract

Leishmania parasites belong to the *Trypanosomatidae* family and are causative agents of leishmaniasis. During their life cycle, *Leishmania* shifts between two different morphological forms, promastigotes (insect vector) and amastigotes (mammalian host). This transition between different hosts entails extensive metabolic adaptations. The identification of pathways that are essential to the parasite and absent from the host is expected to reveal putative drug targets. In this context, the mitochondrion of trypanosomatids is a fascinating organelle showing a number of unique characteristics. These organisms contain a single, elongated and highly branched mitochondrion, unlike most other eukaryotes. Moreover, trypanosomatids mitochondrion houses metabolic pathways required for redox balance and energy production that involve unique enzymes. Two such proteins are directly linked to mitochondrial respiratory metabolism, mitochondrial fumarate reductase (*Li*mFRD) and alternative NADH dehydrogenase (*Li*NDH2). The mFRD enzyme oxidizes NADH reducing fumarate to succinate. On the other hand, NDH2 enzyme catalyzes the oxidation of NADH transferring electrons to ubiquinone. Given the fact that these proteins do not exist in the mammalian host, their potential as therapeutic agents is very promising. The present study aims at understanding the involvement of the *Li*mFRD and *Li*NDH2 enzymes in mitochondrial metabolism of *Leishmania infantum*.

In order to investigate the expression of *Li*mFRD and *Li*NDH2 in *L. infantum*, specific antibodies against each of the proteins were produced. These antibodies detected the respective proteins, *Li*mFRD or *Li*NDH2, in amastigotes and promastigotes developmental stages. Thereafter, the subcellular localization of the proteins was studied. The results obtained by indirect immunofluorescence and protease accessibility upon sequential digitonin solubilization show that both proteins are located in the mitochondrion, *Li*mFRD in the matrix and *Li*NDH2 associated with the inner mitochondrial membrane.

Furthermore, the effects of overexpressing each of these enzymes in energetic metabolism were evaluated by oxygen consumption studies in comparison to the wild type. Overexpression of *Li*NDH2 results in increased basal oxygen consumption with higher activities of complex II and of enzymes that feed electrons into the first entry point of the respiratory chain (including *Li*NDH2). Moreover, the respiratory activity of OE_*Li*mFRD parasites displays decreased sensitivity to KCN, a complex IV inhibitor, probably associated to a higher oxygen consumption that diverged into ROS production by *Li*mFRD. OE_*Li*mFRD basal respiration is similar to that observed in the

wild type strain being sensitive to complex II inhibitors and almost not inhibited by rotenone, an inhibitor of the proton-pumping complex I. Additionally, OXPHOS inhibitors affect growth to the same extent in wt, OE_*Li*mFRD and OE_*Li*NDH2. Interestingly, a specific inhibitor of the alternative oxidase, SHAM, almost completely inhibits *L. infantum* growth.

Further investigations are necessary to have a complete understanding of the involvement of *Li*mFRD and *Li*NDH2 in mitochondrial metabolism in these parasites. The generation of knockout strains for *Li*mFRD and *Li*NDH2 encoding genes as well as the determination of *Li*NDH2 localization will be performed.

Keywords: alternative NADH dehydrogenase; fumarate reductase; NADH oxidation; mitochondria; *Leishmania.*

Resumo

Leishmania é um parasita que pertence à família *Trypanosomatidae e é* o principal agente causador de leishmanioses. Durante o seu ciclo de vida, o parasita transita entre duas formas morfológicas diferentes, promastigota (vetor inseto) e amastigota (hospedeiro mamífero). Esta alteração morfológica requer uma elevada adaptação metabólica por parte do parasita. A identificação de vias fulcrais para o parasita, e que não estejam presentes no hospedeiro, podem ser vistas como promissores alvos terapêuticos. Neste contexto, a mitocôndria dos tripanossomatídeos é um organelo fascinante devido às suas características peculiares e únicas. Estes organismos possuem apenas uma mitocôndria, sendo esta caracterizada pela sua forma alongada e altamente ramificada em oposição à encontrada na maioria dos eucariotas. Além do mais, a mitocôndria dos tripanossomatídeos possui vias metabólicas necessárias para o equilíbrio redox e a produção de energia que envolve enzimas apenas encontradas em alguns organismos. Duas dessas enzimas são a NADH desidrogenase (*Li*NDH2) e a fumarato reductase (*Li*mFRD), que estão diretamente relacionadas com o metabolismo respiratório mitocondrial. A enzima NDH2 tem como função a oxidação de NADH transferindo os eletrões para a ubiquinona. Por sua vez, a mFRD oxida NADH reduzindo fumarato a sucinato. Devido ao facto destas proteínas não existirem no hospedeiro mamífero o seu potencial terapêutico é enfatizado, sendo por isso vistas como promissores alvos terapêuticos. Assim, o presente estudo tem como objetivo perceber o envolvimento das enzimas *Li*NDH2 e *Li*mFRD no metabolismo mitocondrial de *Leishmania infantum*.

De forma a investigar a expressão das proteínas *L*imFRD e *Li*NDH2 em *L. infantum,* produziram-se anticorpos específicos contra cada uma delas. Verificou-se que ambas as proteínas são expressas durante as duas fases de desenvolvimento do parasita. Posteriormente, foi abordada a localização das proteínas recorrendo à imunofluorescência indireta e ensaios de acessibilidade à proteínase K após solubilização com digitonina, concluindo-se que ambas as proteínas se encontram na mitocôndria, *Li*mFRD na matriz e *L*iNDH2 associada com a membrana mitocondrial interna. Seguidamente, foram avaliados os efeitos da sobre-expressão de cada uma das proteínas no metabolismo energético, e, para tal, foram realizados estudos de consumo de oxigénio utilizando as estirpes que sobre expressam cada uma das proteínas comparando o seu fenótipo com o observado na estirpe selvagem. Verificou-se que a estirpe que sobre-expressa a proteína *Li*NDH2 possui um aumento do

consumo de oxigénio basal, registando-se, também, um aumento da atividade do complexo II e de enzimas que fornecem eletrões ao primeiro ponto de entrada de eletrões na cadeia respiratória (incluindo NDH2). Por outro lado, verificou-se que a atividade respiratória dos parasitas OE_*Li*mFRD apresentava uma menor sensibilidade à inibição por KCN, inibidor do complexo IV, o que sugere um maior consumo de oxigénio, para a produção de ROS pela *Li*mFRD. Em relação ao consumo de oxigénio basal verificou-se que a estirpe wt e a OE_*Li*mFRD apresentavam um comportamento semelhante. Foi também avaliado o efeito inibitório da rotenona, inibidor do complexo I, concluindo-se que este não possui efeito sobre as estirpes estudadas. Adicionalmente verificou-se que o efeito dos inibidores da fosforilação oxidativa no crescimento das 3 estirpes em análise wt, OE_*Li*mFRD e OE_*Li*NDH2 é semelhante. De realçar a inibição de crescimento quase total obtida na presença de SHAM, um inibidor específico da oxidase alternativa. Conclui-se que é necessária a realização de mais estudos para perceber qual o papel de *Li*mFRD e *Li*NDH2 no metabolismo mitocondrial destes parasitas, e, para tal, a criação de estirpes mutantes para *Li*mFRD e *Li*NDH2, assim como a determinação da localização exata de *Li*NDH2 são etapas necessárias.

Palavras-chave: NADH desidrogenase alternativa; fumarato reductase; oxidação de NADH; mitocôndria; *Leishmania*.

List of table

Table 1. Primer sequences used for *Li*mFRD and *Li*NDH2 ORF amplification……..….18
Table 2. List of primary and respective secondary antibodies used for western blotting analyses……...22
Table 3. List of primary and respective secondary antibodies used for immunofluorescence analyses……..….23
Table 4. Enzymatic assays composition……...…24
Table 5. Homology between *Li*mFRD and *Li*NDH2 and its respective orthologous proteins from trypanosomatids……...27
Table 6. Basal oxygen consumption in *L. infantum* promastigotes. ……..…45
Table 7. Effect of the respiratory chain inhibitors TTFA and KCN in oxygen consumption.……47
Table 8. Values used for determination of the oxygen consumption rates of the indicated strains.……73

List of figures

Figure 1. Life cycle of *Leishmania spp* 4
Figure 2. Schematic representation of the metabolic pathways of energy metabolism of trypanosomatids 8
Figure 3. Schematic representation of the OXPHOS in *Leishmania* spp……..…10
Figure 4. Recombinant protein expression in *E.coli* BL21CodonPlus. ..... ……..28
Figure 5. Conditions tested to improve the expression of the fusion proteins in the soluble fraction..... …….28
Figure 6. Conditions tested for the improvement in soluble protein yield 29
Figure 7. His_6*Li*mFRD expression in insoluble bodies. 30
Figure 8. Purification of His-tagged *Li*mFRD and *Li*NDH2 by affinity chromatography. 31
Figure 9. His_6*Li*mFRD and His_6*Li*NDH2 purification by preparative gel.. 32
Figure 10. Specificity of α-*Li*mFRD and α-*Li*NDH2 antibodies.. 33
Figure 11. *Li*mFRD and *Li*NDH2 are expressed in axenic amastigotes of *L. infantum* 34
Figure 12. Increasing G418 concentrations does not affect expression of tagged-*Li*mFRD……..….35
Figure 13. Protease accessibility upon digitonin solubilization of wt parasite membranes..... 36
Figure 14. *Li*mFRD is resistant to proteases degradation. 37
Figure 15. Protease accessibility upon digitonin solubilization of OE_*Li*mFRD-cMyc parasite membranes. 37
Figure 16. Localization of *Li*NDH2. 39
Figure 17. Localization of *Li*mFRD. 40
Figure 18. Localization of cMyc tagged-*Li*mFRD. 41
Figure 19. *Li*mFRD is soluble and *Li*NDH2 is found associated with the membrane... 42
Figure 20. OE_*Li*NDH2-cMyc promastigotes respiration. 44
Figure 21. Oxygen consumption by *L. infantum* promastigotes. 45
Figure 22. Oxygen consumption inhibited by TTFA. 46
Figure 23. Oxygen consumption sensitive to KCN and resistant to TTFA..... 47
Figure 24. Inhibition of proliferation of *L. infantum* promastigotes by inhibitors of the OXPHOS 48
Figure 25. Representation of the expression plasmids pET28_6His*Li*mFRD and pET28_6His*Li*NDH2..... 64

Index

Acknowledgements I
Abstract II
Resumo IV
List of tables VII
List of figures VIII
Abbreviations X
Introduction 1
1.1 *Leishmania spp.* 2
1.1.1 Leishmaniasis 2
1.1.2 Life cycle 3
1.2 Carbon metabolism 5
1.2.1 Carbohydrates metabolism 6
1.2.2 Amino acid metabolism 7
1.2.3 Fatty acid metabolism 7
1.3 Mitochondria 9
1.3.1.1 Alternative NADH dehydrogenase 11
1.3.1.2 NADH-dependent fumarate reductase 13
1.4. Drug Development 14
Objectives 15
Materials and Methods 17
3.1 Bioinformatics analysis 18
3.2 Construction of the recombinant vectors 6His*Li*mFRD and 6His*Li*NDH2 18
3.3 Bacterial protein extracts preparation and polyacrylamide gel analysis 19
3.4 Large scale expression of His_6*Li*mFRD and His_6*Li*NDH2 proteins 19
3.5 Purification of His_6*Li*mFRD and His_6*Li*NDH2 proteins 20
3.5.1 Metal ion affinity chromatography 20
3.5.2 Preparative gel 20

3.6 Parasite culture 21
3.7 Parasite protein extracts and western blot analysis 21
3.8 Immunofluorescence 22
3.9 Alkaline carbonate extraction of membrane proteins 23
3.10 Digitonin /proteinase assay 23
3.11 Enzymatic assays 24
3.11.1 Bacterial membrane preparations 24
3.11.2 Parasite membranes preparation 24
3.11.3 Enzymatic assays for NADH:Q_1 oxidoreductase and fumarate reductase 24
3.12 Oxygen Consumption 25
3.13 Effects of inhibitors on *L. infantum* promastigotes growth 25
Results 26
4.1 Expression and purification of His_6*Li*mFRD and His_6*Li*NDH2 proteins 27
4.2 Characterization of the antibodies against *Li*mFRD and *Li*NDH2 32
4.3 Localization of *Li*mFRD and *Li*NDH2 proteins in *L. infantum* 35
4.3.1 Digitonin/proteinase K assay 35
4.3.2 Immunofluorescence 38
4.3.2.1 Localization of *Li*NDH2 38
4.3.2.2 Localization of *Li*mFRD 39
4.3.3 *Li*mFRD is a soluble protein and *Li*NDH2 is associated with the mitochondrial membrane 41
4.4 Enzymatic assays in bacteria and parasite membranes 42
4.5 Oxygen consumption in *L. infantum* 43
4.6 *L. infantum* sensitivity to OXPHOS inhibitors 48
Future work 54
Bibliography 56
Supplementary 63

Abbreviations

ASCT - acetate:succinate CoA-transferase

ATP - adenosine triphosphate

BSA - bovine serum albumin

CCCP - carbonyl cyanide m-chlorophenyl hydrazone

CL - cutaneous leishmaniasis

Cyt c - cytochrome c

DAPI - 4',6-diamidino-2-phenylindole

DIG - digitonin

DNA - deoxyribonucleic acid

DTT - dithiotreitol

EDTA - ethylenediamine tetra-acetic acid

EL - early logarithmic phase

ERC - electron respiratory chain

FAD - flavin adenine dinucleotide

FeS - iron-sulfur

FMN - flavin mononucleotide

FT - flow trough

G3P/DHAP - glycerol 3-phosphate /dihydroxiacetone phosphate

G418 - geneticin

GLB - gel loading buffer

IPTG - isopropyl β-D-1-thiogalactopyranoside

KCN - potassium cyanide

kDa - kilodalton

LB - luria broth medium

***Li*mFRD** - *Leishmania infantum* mitochondrial fumarate reductase

***Li*NDH2 -** *Leishmania infantum* alternative NADH dehydrogenase

***Li*TryS -** trypanothione synthetase

LL - late logarithmic phase

MCL - mucocutaneous leishmaniasis

mTPx - mitochondrial peroxiredoxin

NP-40 - nonidet P-40

OD_{600nm} - optical density

OE - overexpressed

ORF - open reading frame

OXPHOS - oxidative phosphorylation

PBS - phosphate buffered saline

PCR - polymerase chain reaction

PK - proteinase K

PMSF - phenylmethylsulfonyl fluoride

Q_1 - coenzyme Q1

RT - room temperature

SDS - sodium dodecyl sulfate

SHAM - salicylhydroxamic acid

TCA - citric acid cycle

TTFA - thenoyltrifluoro acetone

VL - visceral leishmaniasis

Introduction

Leishmania spp. and *Trypanosoma* belong to the *Trypanosomatidae* family, a large group of flagellated parasitic protozoa that are responsible for diseases in humans and animals. *Leishmania* is responsible for causing different forms of leishmaniasis, the majority in tropical and subtropical regions. On the other hand, *Trypanosoma* spp cause chagas disease in Latin America (*Trypanosoma cruzi*) and human sleeping sickness in Africa (*Trypanosoma brucei*).

Diseases caused by *Leishmania* and *Trypanosoma* currently affect about 22 million people worldwide, and are considered the most important neglected tropical diseases. These parasites have a complex life cycle, alternating between vertebrate and invertebrate hosts. Studies of *Trypanosomatidae* family are now more rapid and efficient upon sequencing of the genome of several of these parasites.

1.1 *Leishmania spp.*

The protozoan parasite of the genus *Leishmania* belongs to the *Trypanosomatidae* family and is the causative agent of leishmaniasis (1). The genus *Leishmania* comprises thirty species of which about twenty are pathogenic to humans (2,3). These parasites are responsible for one of the six most common parasitic infections in tropical regions (4) and its impact on public health is increasing due to the rapid expansion of endemic zones caused, in part, by the increase in global travel (5). This protozoan is responsible for the infection of twelve million people with leishmaniasis, resulting in more than 50.000 deaths each year (3,6,7).

1.1.1 Leishmaniasis

Leishmaniasis is a major and increasing public health problem and comprises a large spectrum of diseases. Inside this spectrum we highlight three general classifications of human leishmaniasis: Cutaneous Leishmaniasis (CL), Mucocutaneous Leishmaniasis (MCL) and Visceral Leishmaniasis (VL), also known as kala-azar. The different types of leishmaniasis have distinct clinic manifestations, for instance, VL causes splenomegaly and hepatomegaly and is fatal if not treated (4). This disease caused by *L. donovani* and *L. infantum* (also designated as *L. chagasi* in South America) represents 90% of the cases registered in the world, being the most affected countries Bangladesh, India, Nepal, Sudan, and Brazil (8). Cutaneous leishmaniasis are localized, self-curing and caused by *L. mexicana* or *L. braziliensis* (1,9). Lastly, MCL lesions can partially or totally destroy the mucous membranes of the

nose, mouth, throat cavities and surrounding tissues and can be caused by different species of *Leishmania* such as *L. braziliensis*, *L. guyanensis* and *L. aethiopica* (1). The different clinical manifestations are due to differences between parasite species, host genetics and immunity factors (2).

1.1.2 Life cycle

Leishmania parasites are pathogens with a complex digenetic life cycle (10). During their life cycle, they shift between mammalian (amastigotes) and insect hosts (promastigotes). In the promastigote form, parasites live within the digestive tract of the sandfly vector where they are elongated and possess a long flagellum, important for its motility and attachment to the sandfly gut (10). Furthermore the so-called promastigote form can include, different stages: procyclic, upon amastigotes return to the promastigote form and metacyclic, representatives of the infective stage (1). In the intracellular amastigote form, parasites live in parasitophorous vacuoles within macrophages (mammalian host); Amastigotes are characterized by its ovoid form and short flagellum that extends to the neck of the flagellar pocket (10,11). Amastigotes proliferate by binary cell division and can spread to other macrophages as well as some to other phagocytic cells (dendritic cells) or even no professional phagocytic cells (fibroblasts) (12). However, it is known that macrophages are the major host cells infected by these parasites (3). Amastigotes are responsible for acute infection, as well as, long term latent infections that can lead to reactivation of the disease years or decades after the primary infections, particularly in immunocompromised individuals (13).

During the life cycle of the parasites, they must adapt to the different environments encountered. These environmental changes lead to a morphological alteration and to a drastic metabolic shift in the parasites. In the transition between the extra- and intracellular environments, the parasite is exposed to alterations such as, elevated temperature, toxic oxidants produced during phagocytosis, acidic pH and proteases encountered in the macrophage phagolysosomes (14). The cycle begins when the mammalian host is infected by flagellated promastigotes that are found within the digestive tract of the sandfly vector. This form of the parasites is transmitted to the mammalian host when a female sandfly injects the parasites into the skin, during its bite. The parasites are rapidly phagocytosed by neutrophils and macrophages, which possess on their surface several glycoconjugates that lead to adherence of promastigotes, and consequently trigger the phagocytic process (15). After phagocytosis, the parasites remain inside the parasitophorous vacuole and develop

into amastigotes. For this, the flagellated promastigotes have to differentiate into amastigotes that are able to live in the acidic pH habitat of the parasitophorous.

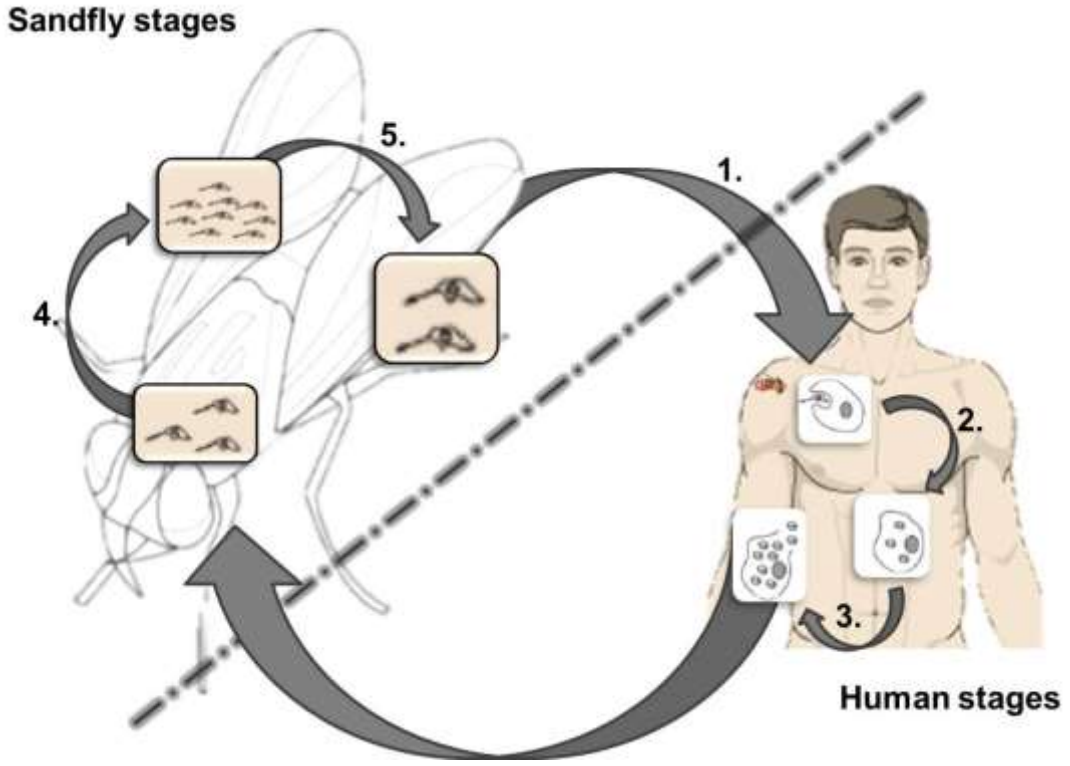

Figure 1. Life cycle of *Leishmania spp*. The numbers shown in figure indicate the different steps in life cycle of the parasite. 1. Promastigotes are injected and phagocytosed by macrophages. 2. Promastigotes become amastigotes inside macrophages. 3. Amastigotes multiply within macrophages in various tissues. 4. Amastigotes differentiate into promastigotes in the midgut. 5. Promastigotes multiply in the midgut and migrate to proboscis.

Then, macrophage lysis occurs caused by a large number of amastigotes resulting from multiple divisions. These free parasites can infect new macrophages or be ingested by sandflies during new blood meals. In sandflies, parasites enter into a differentiation process, where amastigotes transform into procyclic promastigotes, a process known as metacyclogenesis (Figure 1). Upon this, a new infection cycle starts with the differentiation of the non-infective forms into infective metacyclic promastigotes that migrate to the proboscis (1).

Leishmania parasites are auxotrophic or have limited capacity to synthesize de novo a wide range of amino acids, purines, vitamins, lipids and other metabolites that

must, therefore, be available within the parasitophorous vacuole at sufficient levels to permit amastigote growth (3,16,17). Furthermore, the parasites have special organelles that either are absent in eukaryotic organisms, p.e. glycosomes, or have different metabolic pathways (1).

1.2 Carbon metabolism

The study of trypanosomatids carbon metabolism requires a large comprehension about all possible metabolic pathways. The central carbon metabolism of these parasites is necessary for growth, defense against oxidative stress and other host microbicide responses. Alterations, even that partial, may be sufficient to destabilize the synthesis of metabolites essential for viability of the parasite (17).

Trypanosomatids metabolic needs depend partially, if not completely, on the available carbon sources present in their hosts (18). Moreover, these parasites possess distinct characteristics in their metabolism. For instance, the glycolytic pathway is performed in a compartmentalized organelle, the glycosome, unlike in other organisms where glycolysis is accomplished in the cytoplasm (1,19). Furthermore, metabolic alterations between different species and along the life cycle of the parasites also occur (19). For instance, *Leishmania* within the mammalian host live in a habitat with complex nutrient composition due to constitutive internalization of macromolecules and their degradation by lysosomal proteases, lipases and glycosidases. In amastigotes, fatty acids are the main carbon sources used (13) opposing to promastigotes where glycolysis is the main metabolic pathway, thus showing the high adaptation of the parasites to the particular environments (20). Curiously, it was observed that in *Leishmania* most enzymes involved in central carbon metabolism, are constitutively express including those required for the catabolism of glucose, amino acids and fatty acids, even when the carbon sources are limited (13).

The capacity of parasites to adapt to their energetic resources is an advantage for their stability and survival, as demonstrated in the following examples. In trypomastigote forms of *T. brucei* and *T. cruzi,* glucose is predominantly used because it is abundant in the fluids of the vertebrate host. Yet, the insect stage of *T. brucei* can use amino acid catabolism, with preference for L-proline, whereas *T. cruzi* also has the capacity to utilize D-proline in addition to L-proline (18). However, with the exception of *Leishmania,* glucose, when available, is the substrate selected for parasites growth, including for those forms in which glucose is not the natural carbon source. This routinely used carbon source to culture parasites culminated in a better knowledge about glucose metabolism in comparison to amino acid or fatty acid metabolism (18).

Understanding the way parasites produce ATP for their functioning and proliferation through the oxidation of carbohydrates, fatty acids or amino acids is of great relevance.

1.2.1 Carbohydrates metabolism

In trypanosomatids, glucose is degraded to pyruvate using the classical Emden-Meyerhof pathway as in many other organisms (19,20). However, the first reactions of the glycolytic pathway are compartmentalized in modified peroxisomes termed glycosome (Figure 2). The maintenance of the glycosomal redox balance can be achieved either by the production of succinate or by the G3P/DHAP shuttle between glycosomes and mitochondria. The end product of glycolysis, pyruvate, enters the mitochondria and either is completely oxidized through the Krebs cycle or it is converted to acetate. Moreover, pyruvate can also be secreted after transamination to alanine, an essential biosynthetic precursor (18,21).

The tricarboxylic acid cycle (TCA cycle) enzymes are expressed in trypanosomatids where they catalyze the oxidation of acetyl-CoA and are also involved in non-cyclic pathways such as the formation of citrate and succinate and the catabolism of amino acids (22). Studies in *T. brucei* suggest that this non-cyclic function is the main mode of operation of the TCA reactions (23).

In all trypanosomatids, except for the long-slender bloodstream forms of *T. brucei,* glucose metabolism can result in acetate secretion, an end product generated by a two-enzyme cycle involving acetate:succinate CoA-transferase (ASCT) and succinyl-CoA synthetase that also produces adenosine triphosphate (ATP) by substrate level phosphorylation (Figure 2).

The production of glucose by gluconeogenesis is essential for amastigotes virulence and their proliferation inside macrophages, in opposition with the promastigotes that can survive without this pathway (20). Glucose uptake in *L. mexicana* promastigotes was shown to be essential for macrophage infection as evidenced by studies in a mutant that lacks all the glucose transporters. This mutant fails to differentiate into amastigotes in vitro, and thus the hexose requirements in this stage are largely unknown (24).

The capacity of trypanosomes to respond to differences in glucose availability was evaluated. Bloodstream trypanosomes when in a glucose-rich environment express a low affinity transporter with a high capacity for carbohydrate transport. On the other side, *T. brucei* and *T. cruzi* when in a low glucose environment express transporters with high affinity for glucose (25). Furthermore, *T. brucei* in glucose-depleted or limited environment modify their metabolism by increasing L-proline

consumption (26). *Leishmania* and *T. cruzi* are also not dependent on glucose as these parasites have the ability to degrade amino acids in addition to glucose (19).

1.2.2 Amino acid metabolism

Amino acids are also substrates used for energetic metabolism in parasites. In trypanosomatids, the catabolic pathways for many amino acids (glutamate, glutamine, threonine, proline and others) generate intermediates of the Krebs cycle (25,27) that can be completely oxidized or used as biosynthetic precursors in anabolic pathways (Figure 2).

Procyclic *T. brucei* in glucose-depleted conditions uses proline or other amino acids that are catabolized by the TCA cycle. It is known that *Leishmania* promastigotes when in glucose limited conditions also use proline, however, it is not totally clear which catabolic pathway is involved in proline oxidation (6). Other amino acids are used for specific biosynthetic purposes rather than for energy metabolism. For example, arginine and leucine are used for polyamine and sterol/isoprenoid synthesis, respectively (19).

The genome of *Leishmania* encodes a large number of putative amino acid permeases responsible for amino acid uptake and some of them are regulated in a stage-specific manner (28,29).

1.2.3 Fatty acid metabolism

Fatty acids are used as an alternative carbon source by various intracellular pathogens (3). Fatty acids are not considered an important substrate used in energy metabolism of trypanosomatids, however amastigotes of *Leishmania* and *T. cruzi* are exceptions. Thus, it was reported that *L. mexicana* amastigotes have an increase in fatty acid metabolism and a reduction in proline and glucose metabolism (19,20). Actually, β-oxidation appears to be negligible in rapidly dividing promastigotes but increased in non-dividing promastigotes and in axenic amastigotes. Moreover, enzymes involved in fatty acid oxidation are upregulated in *L. donovani* and *L. major* amastigotes (3).

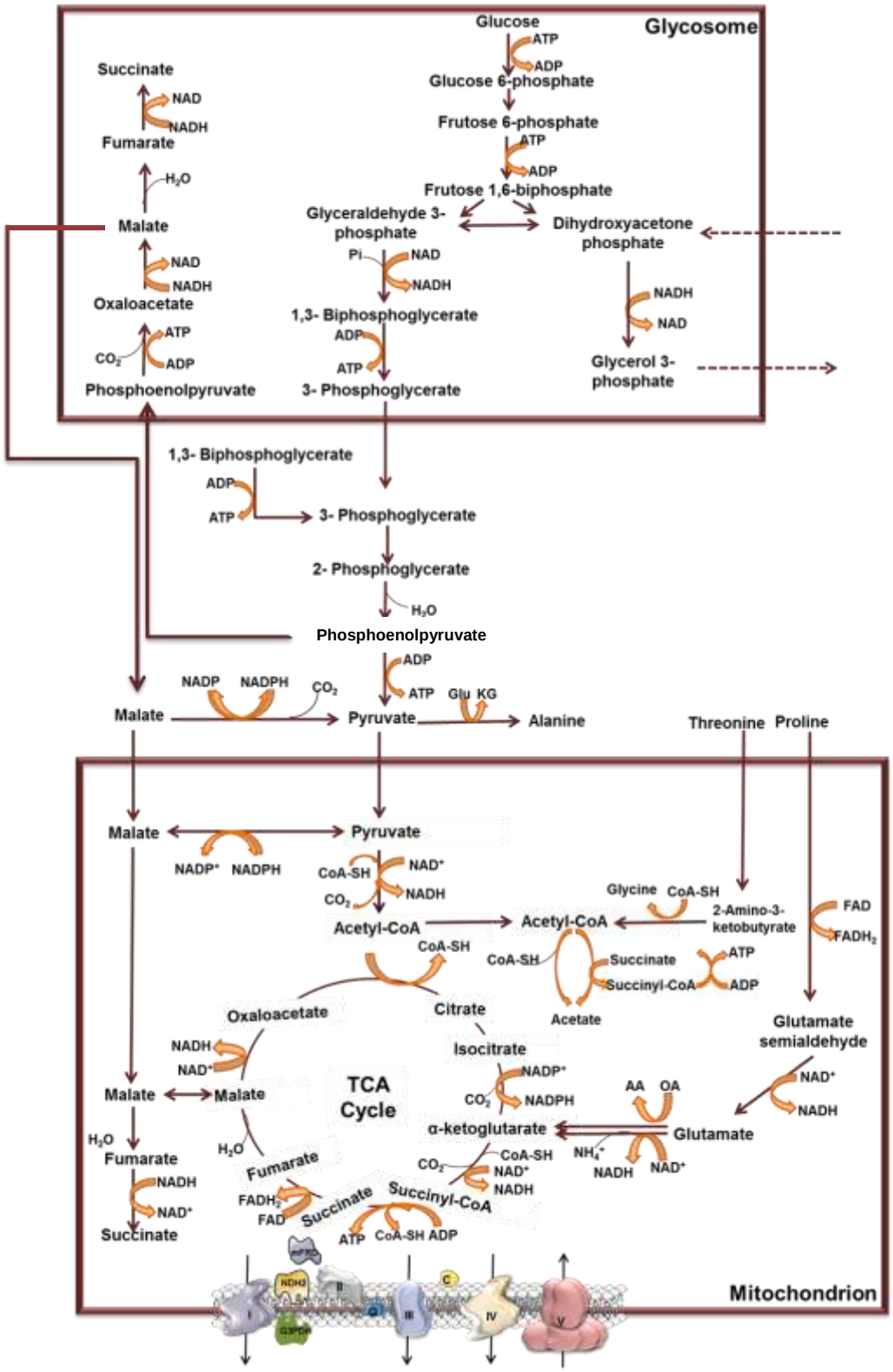

Figure 2. Schematic representation of the metabolic pathways of energy metabolism of trypanosomatids. Adapted from (19).

1.3 Mitochondria

Mitochondria are important organelles, where essential physiological processes occur, such as synthesis and catabolism of crucial amino acids, fatty acid oxidation, iron sulfur cluster biogenesis and oxidative phosphorylation (aerobic organisms) (OXPHOS) (30,31). Catabolic processes result in the production of NADH and occur mainly in the mitochondrial matrix. The NADH formed can be oxidized in the respiratory chain resulting in ATP production through oxidative phosphorylation, the main place where ATP is produced (32). Beyond the metabolic processes, the mitochondrion is involved in other important cell processes, such as programmed cell death, oxidative stress generation and signaling (1).

In trypanosomatids, the mitochondrion is a single and ramified organelle and occupies generally 12% of the protozoan volume (31). As for other organisms, trypanosomatids mitochondrion is constituted by an outer membrane, a dense matrix and an inner membrane that folds into thin and irregularly distributed cristae whose number broadly vary (30). The shape of the organelle varies according to the type of parasite and to its developmental stage (14,31). Moreover, the mitochondrion shape, extension and function changes in response to alterations in the environment thus showing its extreme dynamic capacity. An example often referred about alterations in mitochondrial metabolism, occurs in the electron respiratory chain (ERC) of *T. brucei*. The procyclic form has a complete TCA cycle and a fully functional canonical respiratory chain, while, in the bloodstream form the ERC is extremely different with simpler components involved. Indeed, some trypanosomatids use an alternative oxidase to remove excessive reducing equivalents, instead of the respiratory complexes III and IV. This enzyme is also found in fungi and plants (19). Moreover, ATP production in bloodstream forms occurs mainly by substrate level phosphorylation due to a high glycolytic flux (23). In fact, even in procyclic trypanosomatids growing in glucose-rich medium, mitochondrial ATP synthase has a minor role in ATP production (18). However, the activity of the OXPHOS plays a crucial role in the survival of *Leishmania* amastigotes and promastigotes (8,33).

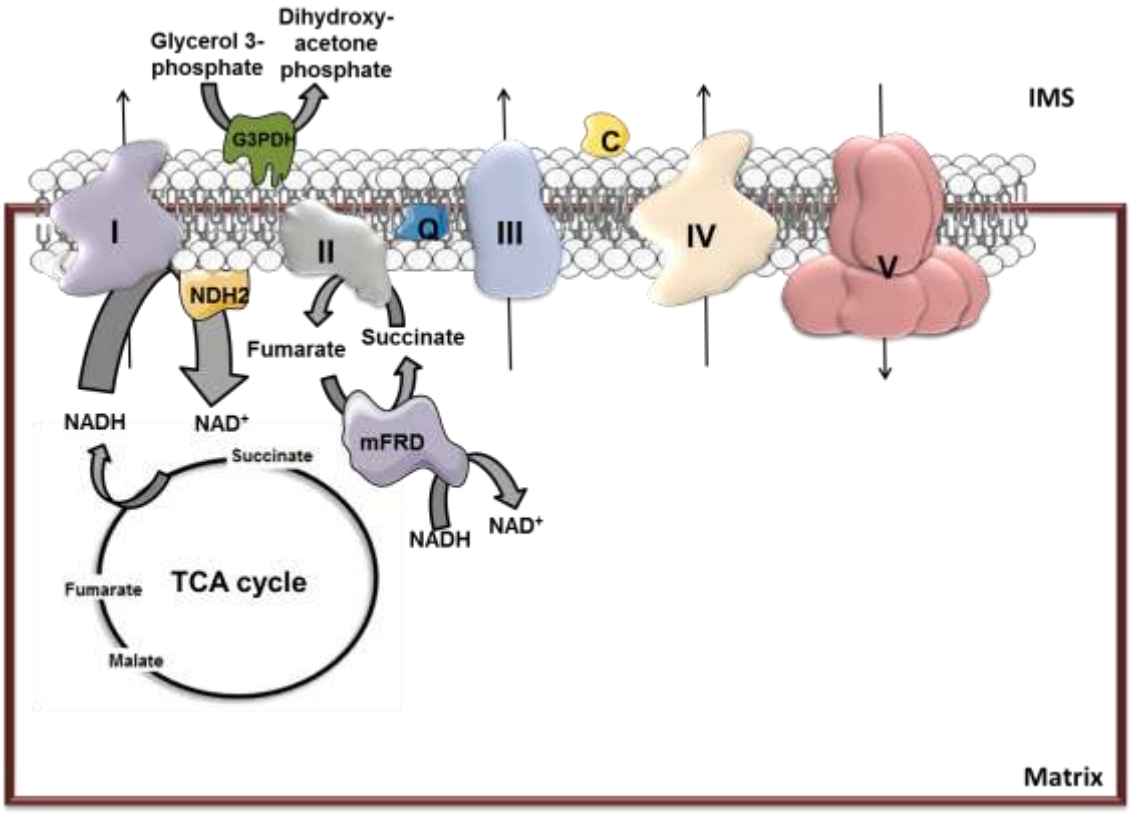

Figure 3. Schematic representation of the OXPHOS in *Leishmania* spp. I,II, III,IV and V refer to the OXPHOS complexes; Q- quinone; NDH2- alternative NADH dehydrogenase; mFRD- mitochondrial fumarate reductase; G3PDH- Glycerol-3-phosphate dehydrogenase.

1.3.1 Electron Respiratory Chain

The canonical electron respiratory chain of eukaryotes is localized in the mitochondrial inner membrane and in its constitution has four different multi-subunit enzymes, designated by respiratory complexes I-IV. NADH dehydrogenase (Complex I), Succinate dehydrogenase (Complex II), cytochrome c reductase (Complex III) and cytochrome c oxidase (Complex IV). These complexes transfer electrons from reduced co-factors produced by catabolic pathways (such as fatty acid oxidation, amino acids and citric acid cycle) to the final acceptor, oxygen. The process where oxygen is consumed is denominated as respiration (8).

Complex I is the first enzyme of the mitochondrial respiratory chain, contains a non-covalently bound FMN molecule and eight iron-sulfur clusters (FeS), and is responsible for the transference of 2 electrons from NADH to ubiquinone (34). Complex II is the smallest respiratory complex and participates in both the TCA and the electron transport chain. This enzyme has covalently bound FAD as well as heme b and donates electrons to ubiquinone reducing it to ubiquinol. Complex III contains heme

and FeS clusters as co-factors and is responsible for the reduction of cytochrome c (cyt c) and oxidation of coenzyme Q. The last enzyme of the respiratory chain, complex IV, receives the electrons from cytochrome c and transfers them to oxygen. Complex I, III and IV use the energy of electron transfer to produce a proton gradient across the mitochondrial inner membrane that is then utilized by F1/F0 ATPase (Complex V) to produce ATP. Complex V along with the ERC constitutes the oxidative phosphorylation machinery (35). The canonical respiratory chain is sensitive to some inhibitors, such as, rotenone, thenoyltrifluoroacetone (TTFA), antimycin A and cyanide, inhibitors of complex I, II, III and IV, respectively (36).

In trypanosomatids the exact constitution of the respiratory chain is unclear, although some evidences exist for the presence of canonical complexes and non-canonical enzymes. In a recent study it was demonstrated that complexes II-IV are present and functional in procyclic *T. brucei*, *T. cruzi*, *Crithidia* and *Leishmania* spp (8,37). *Phytomonas serpens* lacks complexes III and IV and instead expresses an alternative oxidase, as the bloodstream form of *T. brucei* (35,38). Moreover, it was verified that some *Leishmania* spp required OXPHOS for survival in both promastigote and amastigote forms (8,39).

The presence of complex I in trypanosomatids is still an issue that raises much doubt. It was reported that the complex I inhibitor rotenone has low specificity in trypanosomatids, where high concentrations are necessary for complex I inhibition (37,40). More recently, complex I was clearly identified in *P. serpens* and *T. brucei* while in *L. tarentolae* and *C. fasciculata* its presence was not confirmed (35). However, genome mining identifies many genes coding for complex I subunits in the genome of several *Leishmania* spp and *C. fasciculata* (41). The absence of canonical complex I in some trypanosomatids can be compensated by the presence of alternative enzymes able to oxidize NADH, namely alternative NADH dehydrogenase (NDH2) and fumarate reductase (mFRD) (41).

1.3.1.1 Alternative NADH dehydrogenase

The alternative NADH dehydrogenase (NDH2), the so-called rotenone insensitive NADH dehydrogenase, is a single polypeptide chain and contains a non-covalently bound molecule of FAD as cofactor (42,43). These enzymes are characterized by the absence of a transmembrane domain and the presence of two conserved GxGxxG motifs (44). The crystallographic structure of a yeast alternative NADH dehydrogenase shows that it is a monotopic protein interacting with the inner mitochondrial membrane by the C-terminal domain (34). This carboxy-terminal domain

is also critical for the catalytic activity of the enzyme (45). As a monotopic protein, NDH2 can interact with either the external or the internal surfaces of the inner mitochondrial membrane (46), and thus, catalyze the transfer of electrons from the cytosol (external) or matrix (internal) NAD(P)H into the mitochondrial pool of ubiquinone. This electron transfer reaction occurs without proton translocation across the inner membrane, meaning that NDH2 is not associated with the generation of a proton electrochemical gradient, unlike complex I (47).

NDH2 was first identified in plants (48), and then was found in bacteria (49), fungi (50,51) and parasites (52) but its function, in most cases, is not completely understood. Differences in the number and orientation of NDH2 are verified in some organisms where up to five NDH2 enzymes can be present in both the external and the internal faces of the inner mitochondrial membrane (16,43). This enzyme has been extensively studied in various organism namely, *Neurospora crassa (50,51), Solanum tuberosum* (53), *Saccharomyces cerevisiae* (54) and *Mycobacterium tuberculosis (49)*. The filamentous fungus *N. crassa* contains one internal and two external alternatives NADH dehydrogenases in addition to complex I (50). Inhibition of both complex I and the internal alternative NADH dehydrogenase is lethal for the fungus. However, when only one is absent the organism survives, meaning that the internal NDH2 has a complementary function to complex I in *N. crassa* (50). Furthermore, yeasts also possess alternative NADH dehydrogenases where they can co-exist with (*Yarrowia lipolytica*) or without (*S. cerevisiae)* complex I. *S. cerevisiae* possess three alternative dehydrogenases, one internal (NDI1) and two external (NDE1 and NDE2). NDI1 has been suggested to play a role in regulating the redox balance at the level of mitochondrial NADH produced by the citric acid cycle (55), and the external alternative dehydrogenases have an important role in the re-oxidation of the cytosolic NADH produced by glycolysis (56). *Y. lipolytica* contains only one alternative NDH2 enzyme located of the external side in the inner mitochondrial membrane. Complex I in *Y. lipolytica* is essential since the external NDH2 cannot oxidize matrix NADH and thus, compensate for complex I (57). Deletion of the alternative NDH2 did not affect viability or growth rate revealing a non essential role of this enzyme in this yeast (42).

In many protozoa parasites the entry of electrons from NADH into the respiratory chain is made by NDH2 instead of the canonical complex I. *Plasmodium falciparum* expresses one alternative NDH2 (58) and *Toxoplasma gondii* expresses two internal NDH2 enzymes (59). Moreover, a NDH2 enzyme was also identified in *T. brucei* (60) with orthologous proteins predicted in many other trypanosomatids. Depletion of NDH2 in procyclic *T. brucei* decreases the mitochondrial membrane

potential and leads to a significant increase in the activity of G3PDH (61). This phenotype of the knockdown strain allowed the authors to conclude that *T. brucei* NDH2 is a intermembrane space facing enzyme, oxidizing cytosolic NADH (61).

M. tuberculosis and *M. smegmatis* are examples where alternative dehydrogenases have an essential role in growth even in the presence of complex I. Some evidences suggest that NDH2 have an important role in bacteria that preferentially use a non-proton pumping NDH2 instead of the proton-pumping NDH1 when both enzymes are present. The relevance of NDH2 in these bacteria is probably associated with the fact that it is not inhibited by a high proton motive force as is complex I, which could ultimately slow down the metabolic flux due to back-pressure on the system (16).

Alternative NADH dehydrogenases are seen as promising therapeutic targets due to their essential role in many bacterial and eukaryotic pathogens and to their absence in mammalian mitochondria (16,41).

1.3.1.2 NADH-dependent fumarate reductase

The enzyme NADH-fumarate reductase catalyzes the reduction of fumarate, generating succinate, in the presence of NADH (22,62). Multiple forms of fumarate reductases are present in prokaryotes and eukaryotes and they include membrane-bound and soluble proteins (32). The membrane associated enzymes are multi-subunit complexes that performed the reverse reaction of succinate dehydrogenase. The trypanosomatid enzyme is a single polypeptide that uses NADH to reduce fumarate either in the mitochondrion or in glycosomes. These enzymes were characterized in *T. brucei* procyclic forms and orthologues were identified in the genome of *T. cruzi* and *Leishmania* spp (62). The mitochondrial enzyme produces succinate as a final product that can be used by the respiratory chain (complex II) or be excreted into the medium (32,42). FRDs are multifunctional proteins with three different domains, an ApbE domain, a fumarate reductase domain and a cytochrome b5 reductase domain (22,41).

Virginie Cousteau and colleagues described three FRD isoforms in *T. brucei* where two of them are putative mitochondrial proteins and the other is glycosomal. Expression of the proteins was confirmed by western blotting although one of the mitochondrial isoforms is probably not expressed. It was also seen that knockdown of mFRD, but not of gFRD, resulted in a significant cell death at the beginning of the culture. However, after 2-3 days under the induction conditions no cell mortality was observed, suggesting an adaptive compensation of the reduced mFRD expression. The

relevance of these enzymes is recognized when the constitutive knockdown of mFRD or both isoforms failed, indicating an important role of mFRD in the parasite (22).

Moreover, *T. brucei* mFRD was associated with an intracellular production of reactive oxygen species in the absence of fumarate (32). This enzyme is regarded as a promising therapeutic target, since it is absent in mammalian cells. Furthermore, studies with inhibitors of fumarate reductase demonstrate that its inhibition is lethal for trypanosomatids, revealing the importance of this enzyme (32,63).

1.4. Drug Development

Leishmaniasis is a worrying disease owing to the number of people affected and to the fact that no efficient drugs exist. Recently about 25 compounds and formulations were described for the treatment of leishmaniasis (5), however, these drugs continue to have, low efficacy, high toxicity, high expenses and frequently widespread resistance (2). Taking into account the increase number of deaths by leishmaniasis it is urgent the development of novel drugs, for old or new parasite targets, to overcome the parasite multidrug resistance. Searching for new antileishmanial drug targets, we have focused our studies on the electron respiratory chain of *L. infantum* mitochondria (14). Both NDH2 and mFRD are proteins absent in mammalian mitochondria with important roles in the parasite, suggesting that they can be potential drug targets.

Objectives

Leishmaniasis is a neglected disease caused by *Leishmania* spp. and despite the ongoing investigations to find an efficient drug against the disease, a cure is still not available. Current treatments are limited and present several side effects, underlining the importance of developing new drugs. Given that *Li*mFRD and *Li*NDH2 proteins are absent from mammalian mitochondria, these enzymes can be seen as potential drug targets. Thus, this study aims at understanding the involvement of these two NADH oxidizing enzymes, *Li*mFRD and *Li*NDH2, in mitochondrial metabolism of *Leishmania infantum.* To accomplish this goal and thoroughly characterize both enzymes, we:

1) Produced specific antibodies against *Li*mFRD and *Li*NDH2 proteins, using as antigens the recombinant proteins expressed and purified from *Escherichia coli;*

2) Determined the subcellular localization of both proteins in order to elucidate which NADH pool (cytosolic or matrix) is the substrate for these enzymes;

3) Pursued the characterization of the overexpressing strains, OE_*Li*mFRD and OE_*Li*NDH2, in terms of respiratory chain alterations induced by the increased expression of either *Li*mFRD or *Li*NDH2. Moreover, the effect of OXPHOS inhibitors on growth of OE_*Li*mFRD and OE_*Li*NDH2 strains, compared to wild type growth, was evaluated. We expected to identify the metabolic pathways affected by overexpressing either *Li*mFRD or *Li*NDH2.

Materials and Methods

3.1 Bioinformatics analysis

Genome sequence of LinJ.36.5620 and LinJ.35.0850 for *L. infantum* NADH dehydrogenase (*Li*NDH2) and *L. infantum* mitochondrial fumarate reductase (*Li*mFRD) respectively were obtained at the Kinetoplastid Genome Resource: TriTrypDB. Amino acid sequences alignment was carried out with the BLAST software.

3.2 Construction of the recombinant vectors 6His*Li*mFRD and 6His*Li*NDH2

For the construction of pET28_6His*Li*mFRD and pET28_6His*Li*NDH2, *Li*mFRD and *Li*NDH2 open reading frames (ORF) were amplified with *Pfu* Turbo DNA polymerase (Stratagene) using primers described in table 1.

Table 1. Primer sequences used for *Li*mFRD and *Li*NDH2 ORF amplification. Restriction sites are underlined in the sequences and clamp sequences are in lowercase.

Primer	*Li*mFRD	*Li*NDH2
Forward	5´ccgcgcaCATATGGCCACCG CGAGCTTCGTGA-3´	5´ccgcgcaCATATGCTGCGCAGCAC GTTGCG-3´
Reverse	5´gggAAGCTTGAGTCATTTG GCCGACTGC-3´	5´-caccgCTCGAGCTACATTTTCTTTTC GGGTTC-3´

PCR products obtained for *Li*mFRD and *Li*NDH2 were cloned, respectively, between *Nde*I/*HindIII* and *Nde*I/*Xho*I restriction sites of the pET28 expression vector (Novagen) in frame with a N-terminal 6His-tag. pET28_6His*Li*mFRD and pET28_6His*Li*NDH2 plasmids were transformed into *Escherichia coli* DH5α strain competent cells and plasmid DNA was extracted using Genelute plasmid miniprep kit (Sigma Aldrich). For fusion protein expression, each of the plasmids was introduced into *E.coli* BL2I, BL21CodonPlus and Rosetta competent cells. Correct DNA sequence was confirmed by sequencing analysis.

3.3 Bacterial protein extracts preparation and polyacrylamide gel analysis

E. coli BL2I, BL21CodonPlus and Rosetta with plasmid pET28_6His*Li*mFRD or pET28_6His*Li*NDH2 were grown overnight in Luria broth media (LB) supplemented with kanamycin (50 µg ml^{-1}) at 200 rpm, 37ºC. After this, bacteria were diluted 1.5:100 in LB and grown at 37ºC and 150 rpm until 0.5-0.9 Optical Density at 600nm (OD_{600}). Then, protein expression was induced with 0, 0.1, 0.25 or 0.5 mM isopropyl-β-D-galactopyranoside (IPTG), at 25ºC during 5 hours. Protein extracts from 3 ml bacterial culture were obtained by pelleting (775g , 10 min) and further processing by sonication using a Branson sonifier (5x10 seconds on ice). Lysates were then centrifuged (16873g, 10 min) in order to fractionate the samples. Afterwards, supernatant (soluble) and pellet (membrane plus insoluble) fractions were resuspended in gel Loading Buffer (50 mM Tris-HCl pH 6.8, 2% (w/v) SDS, 0.1% (w/v) bromophenol blue, 10% (w/v) glycerol and 2% (v/v) β-mercaptoethanol) (GLB) and boiled for 10 minutes at 95 ºC. The different fractions were loaded into a 10% SDS-PAGE gel and after running was completed the gel was stained with coomassie blue (0.1% Coomassie Blue R250 in 10% (v/v) acetic acid, 50% (v/v) ethanol).

3.4 Large scale expression of His_6*Li*mFRD and His_6*Li*NDH2 proteins

His_6*Li*mFRD and His_6*Li*NDH2 proteins were induced as described above in 500 ml culture. Subsequently, bacteria were centrifuged for 20 min at 9150g, 4ºC. Collected pellets were washed once and resuspended in phosphate buffered *saline* (PBS), always on ice. The resulting suspension was sonicated (5x10 seconds on ice) and centrifuged, for 30 minutes at 26700g, 4ºC. Aliquots of pellets and supernatant fractions were resuspended in GLB and boiled for 10 minutes at 95 ºC and loaded into a 10% SDS-PAGE gel that was stained with coomassie blue to check for protein expression.

3.5 Purification of His_6*Li*mFRD and His_6*Li*NDH2 proteins

3.5.1 Metal ion affinity chromatography

Fresh induced bacterial pellets were resuspended in Buffer A (20 mM Tris-HCl, 500 mM NaCl, 5mM imidazole, pH 7.6), sonicated (10x10 seconds on ice) and then centrifuged for 20 min at 26700g, 4ºC. The supernatant was loaded into a Histidine Bind resin (HiTrap, GE Biosciences) column, previously equilibrated with Buffer A without imidazole. Alternatively, the pellet was solubilized with Buffer A+8 M urea for 1 h at room temperature (RT), centrifuged as described above and the supernatant was applied into a Histidine Bind resin equilibrated with Buffer A+8 M urea. The collected flow through was reloaded at a flow rate of 1.5 ml min^{-1} in order to improve the purification yield. Elution was carried out by a linear imidazole gradient through increased Buffer B (20 mM Tris, 0.5 M NaCl and 1 M imidazole). Furthermore, several purification conditions were evaluated by adding different compounds, namely SDS, urea, Triton X-100 and dithiothreitol (DTT) to both Buffers A and B in order to improve the process efficiency.

3.5.2 Preparative gel

For this procedure, fresh induced bacterial samples were prepared. His_6*Li*mFRD and His_6*Li*NDH2 expressed in *E.coli* inclusion bodies were washed with 2 M urea followed by a 3 M urea wash in Buffer A and then solubilized with 8 M urea for 1h at RT. Supernatants of 8 M urea incubation were precipitated with 20% (w/v) trichloroacetic acid, incubated 20 minutes on ice and centrifuged for 10 minutes at 16873g, 4ºC. Pellets were washed with acetone, vortexed and immediately centrifuged as previously described. Precipitates were dried at RT, resuspended in loading buffer (50 mM Tris pH 8.8, 2% SDS (w/v), 10% glycerol, 2 mM EDTA, 0.02% (w/v) bromophenol blue, 5% (w/v) DTT) and heated at 65ºC for 10 min. Processed samples were then loaded into a 15 % polyacrylamide gel (30% acrylamide/bis acrylamide (37.5:1); 1.875 M Tris-HCl pH 8.8; 10% SDS (w/v); Temed; 10% APS (w/v)) and run with the specific buffers: upper buffer (1.5 mM Tris; 9.4 mM glycine; 0.1% SDS; 0.12 mg/ml coomassie R250) and lower buffer (1.5 mM Tris; 9.4 mM glycine; 0.1% SDS) at 30 mA for 4 hours.

After gel running, the selected bands were excised from the stained gel with a blade, crushed with a syringe and incubated overnight in 20 ml of 0.02% SDS, 5 mM DTT solution. After protein extraction, suspension was centrifuged and the resulting supernatant was collected and rapidly frozen with a mixture of dry ice and 70% ethanol. The resulting samples were lyophilized to reduce volume and then precipitated with 80-90% acetone and incubated overnight at -20ºC. After this, samples were centrifuged and the pellets resuspended in PBS. This material was sent to animal facility (IBMC) for rat immunization.

3.6 Parasite culture

Leishmania infantum promastigotes derived from the MHOM/MA/67/ITMAP-263 were cultured at 26ºC (BK 4062, EHRET) in RPMI 1640 medium with glutaMAX (Invitrogen) supplemented with 10% heat-inactivated fetal bovine serum (FBSi, Invitrogen), 20 mM HEPES sodium salt buffer (Sigma) pH 7.4, 50 U ml^{-1} penicillin and 50 µg ml^{-1} streptomycin (Gibco). The transfected *L. infantum* promastigotes were cultured in the presence of 15 µg ml^{-1} Geneticin (G418).

3.7 Parasite protein extracts and western blot analysis

Protein extracts were prepared from cultures of *L. infantum* promastigotes and axenic amastigotes. Initially, $5x10^6$ cells were pelleted by centrifugation for 10 min at 3000 rpm, washed with PBS and lysed with 8 µl 50 mM Tris-HCl pH 7.6, 4% SDS solution, then 10 µl PBS and 5 µl 5xGLB were added. Cells were then gently vortexed, incubated for 10 minutes at 65 ºC and loaded into a 10% SDS-PAGE gel. Afterwards, the proteins were transferred onto a nitrocellulose Hybond-C Extra membrane (GE Biosciences), the membrane was incubated in a blocking solution of 5% skim milk in TBS-T (20 mM Tris-HCl, 137 mM NaCl, 0.1% Tween 20, pH 7.6) during 1 hour, followed by incubation with primary antibodies (shown in table 2). Membranes were then washed 3 times 5 minutes each with TBS-T and incubated with secondary antibodies for 1 hour. After washing as described above, membranes were revealed using Clarity^{tm} western ECL substrate (BIO-RAD) chemiluminescence kit to detect the bands. The images were acquired using image lab software (Biorad).

Table 2. List of primary and respective secondary antibodies used for western blotting analyses.

Primary antibody	Secondary antibody
α- *Li*NDH2 (1:1000)	α- rat(1:4000)
α- *Li*mFRD (1:1000)	
α- *Li*ZIP1(1:1000)	
α- cMyc (1:100)	α- mouse (1:5000)
α- mTPX (1:1000)	α- rabbit(1:10000)
α- GAPDH (1:1000)	
α- *Li*TryS (1:1000)	
α- arginase (1:100)	

3.8 Immunofluorescence

L. infantum promastigotes were collected and washed once with PBS. Parasites were fixed during 10 minutes in 4% (w/v) formaldehyde in PBS at RT and then centrifuged for 5 min at 775g, 4ºC. Pellets were washed, ressuspended in PBS and placed onto polylysine slides previously smeared. Parasites were left to dry for 15-20 minutes at 45ºC, rehydrated with PBS and incubated with 0.1 M glycine in PBS for 15 minutes at RT. After this, cells were permeabilized with 0.05 M glycine, 0.1% (w/v) Triton X-100 in PBS for 8-9 minutes at RT, followed by several washes with PBS. Then, cells were blocked for 30-60 minutes with 1% (w/v) bovine serum albumin (BSA) at RT, and incubated in a humid chamber with the primary antibody (shown in table 3) for 1 hour at RT. Afterwards, the slides were washed and then incubated in a humid dark chamber with the respective secondary antibody during 1 hour at RT. The excess secondary antibody was removed with PBS and cells were incubated with 5 µg ml^{-1}, 4',6-diamidino-2-phenylindole (DAPI) for 15 min. Slides were immediately mounted with 60% glycerol and visualized in a Zeiss Axio Imager Z1 microscope (Carl Zeiss). Images were acquired using the AxioVision Rel. 4.8 software (Carl Zeiss).

Table 3. List of primary and respective secondary antibodies used for immunofluorescence analyses.

Primary antibody	Secondary antibody
α- *Li*NDH2 (1:500)	Alexa Fluor 488 α-rat (1:2000)
α- *Li*mFRD (1:500)	Alexa Fluor 488 α-rat (1:2000)
α- mTPX (1:1000)	Alexa Fluor 468 α-rabbit (1:2000)
α- cMyc (1:100)	Alexa Fluor 488 α-mouse (1:2000)

3.9 Alkaline carbonate extraction of membrane proteins

Logarithmically growing cells were harvested, washed twice with PBS and resuspended in a freshly made 0.1 M Na_2CO_3 pH 7.4 solution at final concentration $1x10^8$ parasites ml^{-1}. After this, cells were disrupted by sonication (10x10 seconds on ice) and incubated for 20 minutes on ice. After incubation, the suspension was centrifuged (Optimal^{tm} L-80 XP ultracentrifuge, Beckman Coulter) for 75 minutes at 100.000g, 4ºC. The pellet was resuspended in GLB and the supernatant was incubated during 30 minutes with 10% trichloroacetic acid on ice. After precipitation, the supernatant was centrifuged for 15 minutes at 16873g, 4ºC. The resulting pellet was washed with acetone, centrifuged as described above, dried and resuspended in GLB.

3.10 Digitonin /proteinase assay

Three days culture (logarithmic culture) parasites were centrifuged at 775g for 10 min at RT. The pellet was washed twice with PBS and resuspended in digitonin (DIG) buffer (25 mM Tris-HCl, pH 7.8; 1 mM EDTA; 0.6 M sucrose; 1 mM E-64; 5 mM pepstatin; 1mM PMSF) at a final concentration of $2x10^9$ parasites ml^{-1}. Equal volumes of parasites ($1x10^7$) were incubated on ice for 3 minutes with different digitonin concentrations 0, 0.0625, 0.25, 0.75, 1.0, 1.5 and 2.5 mg per mg of protein. Then, 15 volumes of DIG buffer were added to each sample in order to stop membrane solubilization. After this, 30 µg ml^{-1} of proteinase K (PK) were added and incubated during 20 minutes on ice. The PK reaction was terminated by addition of 2 mM phenylmethylsulfonyl fluoride (PMSF), during 5 minutes on ice. Then, samples were precipitated with 10% (w/v) trichloroacetic acid, incubated for 30 minutes on ice and centrifuged for 10 minutes, at 16873g, 4ºC. The pellet was washed with acetone, dried

at RT and resuspended in GLB with 5% β-mercaptoethanol. The protein fractions were analyzed by western blot.

3.11 Enzymatic assays

3.11.1 Bacterial membrane preparations

Bacteria expressing either His_6*Li*mFRD or His_6*Li*NDH2 were centrifuged for 20 minutes at 9150g, 4ºC and the pellet was resuspended in solution 1 (50 mM Tris-HCl pH 8.0, 1 mM EDTA, 1 mM PMSF). Suspension of bacteria was disrupted by cell cracker emulsiflex C5 (Avestin) and centrifuged for 25 min at 26700g, 4ºC. The supernatant was centrifuged (Optimal^{tm} L-80 XP ultracentrifuge, Beckman Coulter) for 75 minutes, 100.000g at 4ºC and the resulting pellet resuspended in solution 2 (50 mM Tris-HCl pH 8.0, 1 mM EDTA, 200 mM NaCl, 1 mM PMSF and 10% glycerol). Membranes were homogenized and protein concentration was determined using Pier(R) BCA Protein Assay (Thermo scientific).

3.11.2 Parasite membranes preparation

Logarithmic parasites ($1x10^8$) were pelleted and washed with PBS. Subsequently, pellets were resuspended in 500 µl 1xSoTE (20 mM Tris-HCl pH 7.5, 0.6 M sorbitol, 2 mM EDTA) and 500 µl 0.06% (w/v) DIG in 1xSoTE were gently added. The tubes were inverted 2 times and incubated on ice during 5 minutes. Then, samples were centrifuged for 5 minutes at 5510g (Eppendorf, Centrifuge 5418), 4ºC. Pellet was washed with SoTE (without resuspension) and centrifuged, as mentioned above. Lastly, pellet was carefully resuspended in 200 µl 1x SoTE.

3.11.3 Enzymatic assays for NADH:Q_1 oxidoreductase and fumarate reductase

Table 4. Enzymatic assays composition.

NADH:Q_1	**NADH:Fumarate**
1.5 ml 50 mM KPP pH 7.1	
1 mM KCN	
250 µM NADH	
60 µM Q_1	1 mM Fumarate

The consumption of NADH was measured at 340 nm, at 25ºC or 37ºC using a spectrophotometer Shimadzu UV-2041 PC. The reaction was monitored during 300 seconds.

3.12 Oxygen Consumption

L. infantum promastigotes cultured at 1.4-2.0 $x10^7$ parasites ml^{-1} were centrifuged, washed with PBS and resuspended to a final concentration of $2x10^8$ ml^{-1}. Oxygen uptake with intact parasites was measured polarographically at RT with a Clark-type oxygen electrode (Hansatech). The assays started with the addition of 0.10-0.4 mg (1.5-6 x $x10^7$ parasites) of protein to the reaction medium containing 0.3 M sucrose, 10 mM potassium phosphate pH 7.2, 5 mM $MgCl_2$, 1 mM EGTA, 10 mM KCl, 4 µM carbonyl cyanide m-chlorophenylhydrazone (CCCP), and 0.02% (w/v) BSA. During the assay, different substrates and inhibitors were added to the reaction. The substrates used were 5 mM succinate or 3 mM L-proline and the inhibitors were 2 mM TTFA, 60 µM rotenone and 1 mM KCN. Results were evaluated with O2view software (Hansatech).

3.13 Effects of inhibitors on *L. infantum* promastigotes growth

Parasites at $1x10^6$ ml^{-1} final concentration were inoculated in 24- well plates with RPMI in the presence of different respiratory chain inhibitors. The plate was incubated for 3 days at 26 ºC. The concentrations of the inhibitors tested were 1 mM for KCN, 20 and 60 µM for rotenone, 2 mM for TTFA, 2 µg ml^{-1} for antimycin, and 2 µg ml^{-1} for oligomycin and 0.5, 1.0 and 5.0 mM for Salicylhydroxamic acid (SHAM). Afterwards, growth was monitored through microscope visualization. The final result of inhibition was evaluated by measuring OD_{600nm} using a spectrophotometry (UV-VIS spectrophotometer, Shimadzu).

Results

In this work we investigate two proteins involved in mitochondrial metabolism of *Leishmania infantum*, namely: mitochondrial fumarate reductase (*Li*mFRD) and the alternative NADH dehydrogenase (*Li*NDH2). The amino acid sequences of *Li*mFRD and *Li*NDH2 (LinJ.35.0850 and LinJ.36.5620, respectively) were obtained from the Kinetoplastid Genome Resource: TriTrypDB. *Li*mFRD and *Li*NDH2 encode proteins with a theoretical molecular weight of 129.7 and 57.5 kDa, respectively. These proteins are highly homologous to proteins present in other organisms belonging to the *Trypanosomatidae* family, as shown in table 5.

Table 5. Homology between *Li*mFRD and *Li*NDH2 and its respective orthologous proteins from trypanosomatids. The percentage of identity was determined upon alignments performed with BLAST software using sequences obtained from TriTrypDB database. The access number of the proteins used is: XP_003864671.1, XP_003879080.1, EKF32293.1, XP_822614.1 and CCW64868.1 for *Li*mFRD homologues and XP_003865675.1, XP_003874897.1, EKG04215.1, XP_823167.1 and CCW63333.1 for *Li*NDH2 homologues, from *L. donovani*, *L. mexicana*, *T. cruzi*, *T. brucei* and *Phytomonas*, respectively.

	L. donovani	***L. mexicana***	***T. cruzi***	***T. brucei***	***Phytomonas***
*Li*mFRD	99	95	63	60	52
*Li*NDH2	99	97	62	62	65

4.1 Expression and purification of His_6*Li*mFRD and His_6*Li*NDH2 proteins

Expression and purification of His_6*Li*mFRD and His_6*Li*NDH2 proteins was performed in order to produce antibodies against these polypeptides. To accomplish this objective we started with the production in large scale of the two proteins. For this purpose, *Li*mFRD and *Li*NDH2 ORF were separately cloned into pET28 expression vector, generating, pET28_6His*Li*mFRD and pET28_6His*Li*NDH2, respectively. Subsequently, insertion of a correct sequence in the vector was confirmed by complete sequencing and *E. coli* BL2I, BL21CodonPlus and Rosetta bacteria were transformed with these plasmids. Expression of the fusion proteins was performed by growing bacteria at 37ºC (temperature normally used for induction tests), during 8 hours following IPTG induction.

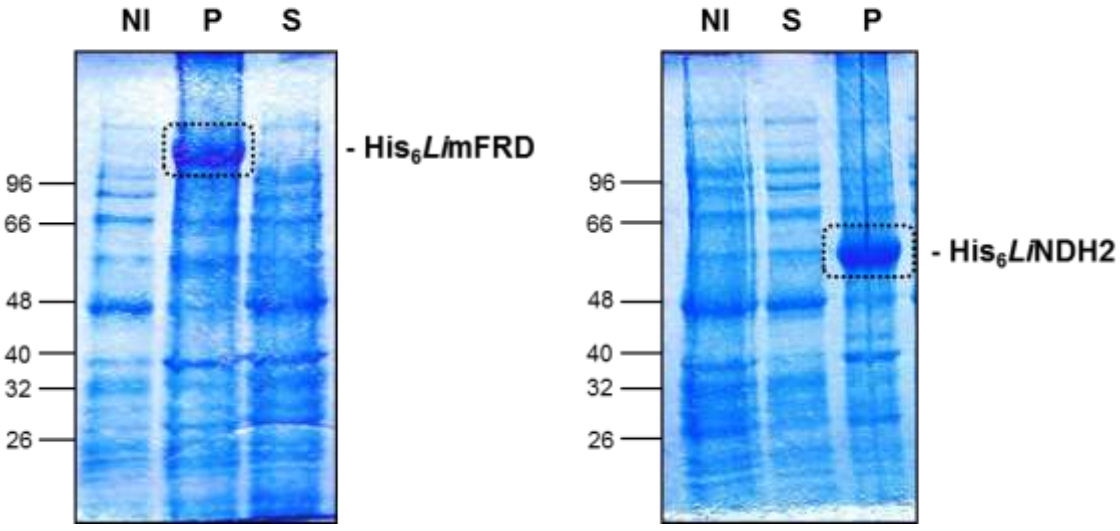

Figure 4. Recombinant protein expression in *E.coli* BL21CodonPlus. Expression of His_6*Li*mFRD and His_6*Li*NDH2 was analyzed by SDS-PAGE stained with coomassie blue. Protein from total extracts of non-induced (NI), pellet fractions (P) and supernatant fractions (S) were loaded. The position of the recombinant proteins is indicated.

As shown in figure 4, both proteins were successfully expressed with the expected molecular weight, 129.7 kDa and 57.5 kDa for His_6*Li*mFRD and His_6*Li*NDH2, respectively. In both cases no protein was observed in the non-induced extracts (NI), but following addition of 0.1 mM IPTG (inducing agent) protein expression is observed and it is predominantly present in the pellet fractions (P). These observations indicate that proteins are found either in the membrane or in insoluble forms. In order to try to express His_6*Li*mFRD and His_6*Li*NDH2 in the soluble fraction of bacteria, we investigated the effect of several expression conditions such as concentration of IPTG, growth temperature, addition of different soluble compounds to the growth media and activation of chaperones, as summarized in figure 5.

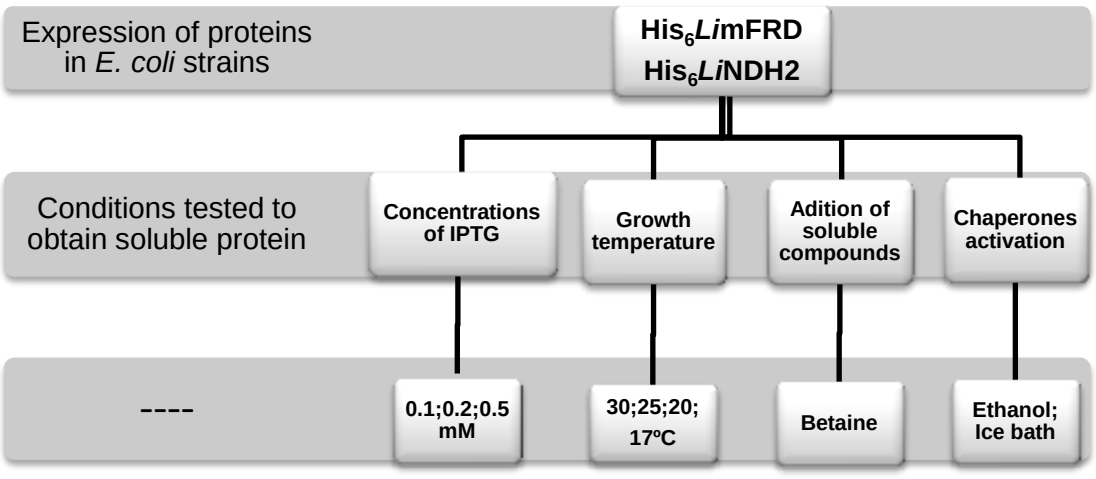

Figure 5. Conditions tested to improve the expression of the fusion proteins in the soluble fraction.

The results obtained were not encouraging, as seen in figure 6, with no significant increase in the amount of His_6*Li*mFRD and His_6*Li*NDH2 as soluble proteins.

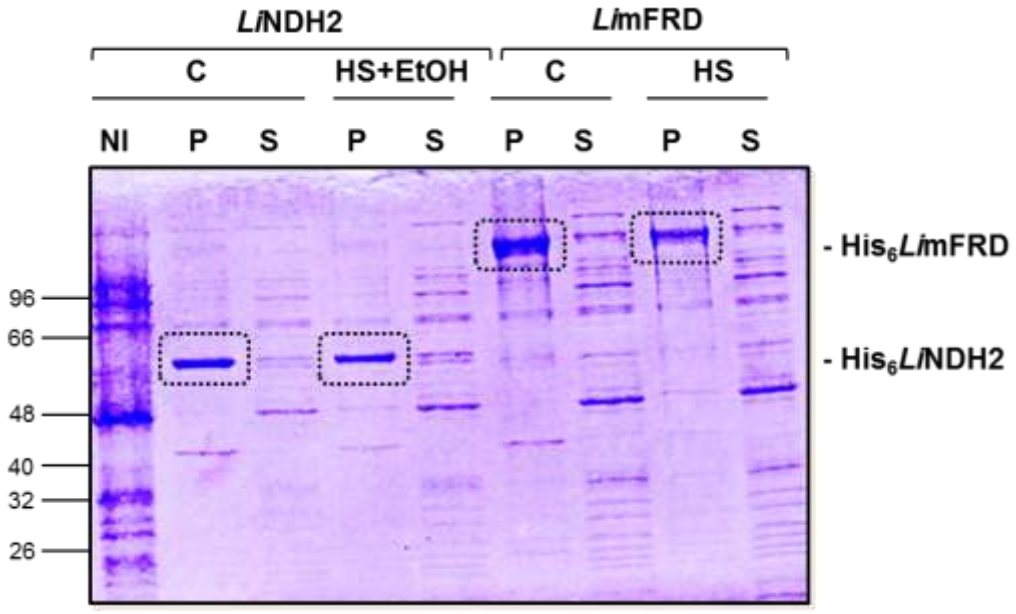

Figure 6. Conditions tested for the improvement in soluble protein yield. *E.coli* expressing either His_6*Li*mFRD or His_6*Li*NDH2 were grown under normal conditions (C) or subjected to 30 minutes cold shock (HS) or 30 minutes cold shock plus 10% Ethanol (HS+EtOH), as indicated. Bacteria were fractionated into pellet (P) and supernatant (S) and resolved by SDS-PAGE. The gel was stained with coomassie blue.

In the experiment shown in figure 6, the condition tested for the improvement in His_6*Li*mFRD expression was thermal shock before IPTG induction. In the case of His_6*Li*NDH2, the same condition was tested, as well as the addition of 10% ethanol to the bacterial culture prior to thermal shock. Both conditions will lead to chaperones activation increasing the probability of correct folding of the overexpressed proteins. Unfortunately, when we compare the expression of the fusion proteins with the respective expression controls, grown in normal conditions (without thermal shock and ethanol addition), we see similar results with no protein or a very low amount in the soluble fractions. Nonetheless, the soluble fractions of *E. coli* overexpressing strains were used in affinity chromatography purification process. No recombinant proteins were purified probably due to an insufficient amount of soluble protein. In light of these results, a new strategy was adopted taking advantage of the high amount of recombinant protein expressed in inclusion bodies (see figure 4). We cultured bacteria in large scale, fractionated them into pellet and supernatant and washed the inclusion bodies (pellets) with increasing concentrations of urea as a way to decrease contamination by other proteins (figure 7).

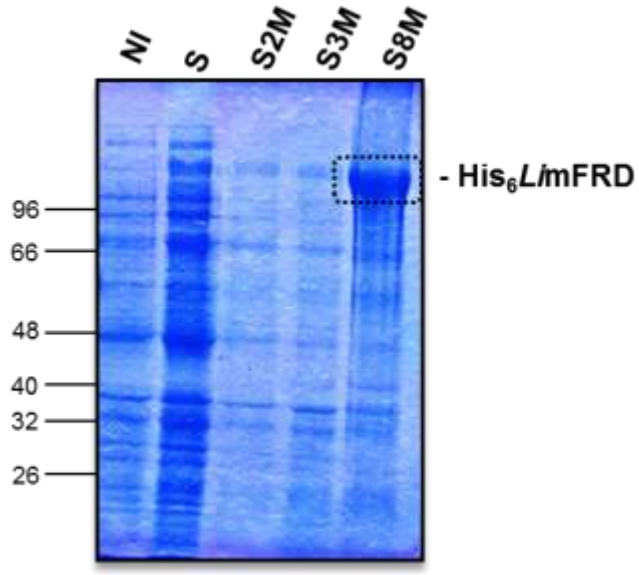

Figure 7. His$_6$*Li*mFRD expression in insoluble bodies. Protein extracts from non-induced (NI), supernatant (S), and supernatants resulting from consecutive washes with 2, 3 and 8 M urea (S2M, S3M and S8M) were resolved by SDS-PAGE and the gel was stained with coomassie blue.

We found, firstly, His$_6$*Li*mFRD was successfully induced, secondly our protein is soluble in 8 M urea and lastly contaminants were removed with increasing urea concentration washes (2M and 3M). The same protocol was used for His$_6$*Li*NDH2 (data not shown). The S8M supernatant was applied to an affinity chromatography column and the purification results can be seen in the chromatogram of figure 8 and in the respective SDS-PAGE analysis.

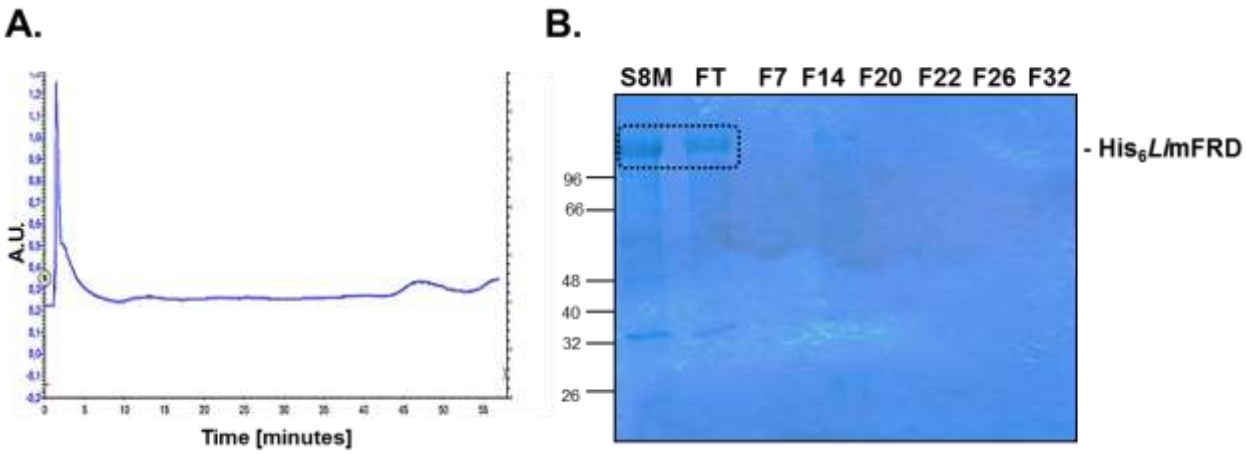

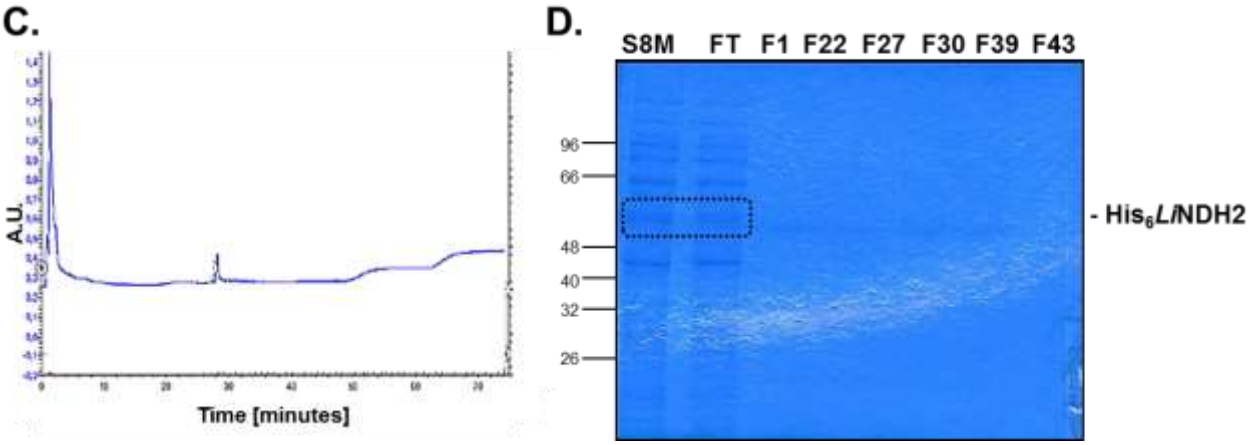

Figure 8. Purification of His-tagged *Li*mFRD and *Li*NDH2 by affinity chromatography. A and C illustrate chromatograms obtained by affinity chromatography for His_6*Li*mFRD and His_6*Li*NDH2 purification, respectively. B and D show SDS-PAGE analysis of the indicated fractions of the column purification. Sample loaded in column (S8M); flow through (FT); Fractions collected in the purification (F1, F7, F14, F20, F22, F26, F27, F30, F32, F39, F43).

As shown in figure 8, no His_6*Li*mFRD protein was purified. An absorbance peak was expected after increasing imidazole concentrations in the elution buffer, however this was not observed. Analysis of the His_6*Li*NDH2 chromatogram showed the same result. These observations were corroborated by SDS-PAGE analysis of several fractions of the purification procedure showing that most of the protein is present in the flow through (FT). The fact that the majority of the fusion protein is present in the FT means that the protein does not bind or binds weakly to the column in the conditions used. Therefore, we altered the procedure conditions by changing buffer composition including, urea, DTT, Triton X-100 or SDS. However, none of these attempts improved the yield of purified proteins.

After all the unsuccessful attempts referred to above, we decided to change the protein purification strategy. In this case, the two proteins, His_6*Li*mFRD and His_6*Li*NDH2, were purified using a preparative gel. For this we expressed the recombinant proteins as inclusion bodies, washed them with increasing urea concentrations and solubilized the final pellets with 8 M urea before gel separation, according to the protocol described in materials and methods. Afterwards, the purity of the samples was confirmed by SDS-PAGE, as shown in figure 9.

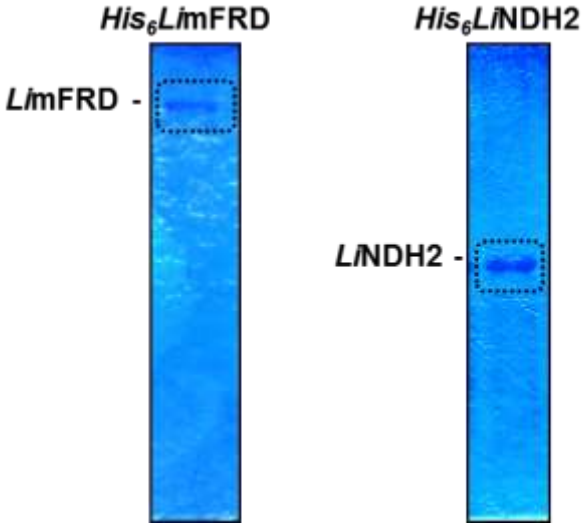

Figure 9. His$_6$*Li*mFRD and His$_6$*Li*NDH2 purification by preparative gel. SDS-PAGE analysis of the final protein samples upon preparative gel purification. The gel was stained with coomassie blue.

Both proteins were purified successfully by this method, with no visible contaminants. This material was used to immunize rats in order to produce antibodies against His$_6$*Li*mFRD and His$_6$*Li*NDH2.

4.2 Characterization of the antibodies against *Li*mFRD and *Li*NDH2

In order to study the specificity of the antibodies α-*Li*mFRD and α-*Li*NDH2 against *L. infantum,* total protein extracts were analyzed by Western Blot. In this experiment we used the *E. coli* His-tagged recombinant proteins as positive controls, and samples from different growth stages of *L. infantum* promastigotes from the wild type, the OE_*Li*mFRD-cMyc and the OE_*Li*NDH2-cMyc strains (figure 10). Parasites from wt were transformed with multi-copy recombinant plasmids that lead to overexpression of either *Li*mFRD or *Li*NDH2 proteins generating strains OE_*Li*mFRD-cMyc and OE_*Li*NDH2-cMyc, respectively. These plasmids confer resistance to G418 and varying the drug amount we can modulate the overexpression of cMyc tagged *Li*mFRD and *Li*NDH2 proteins.

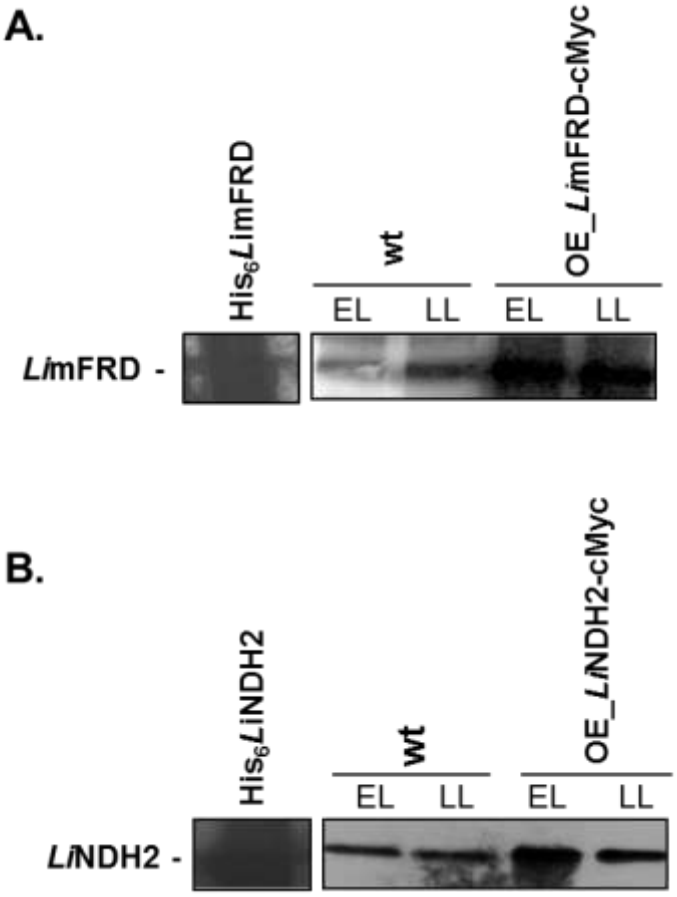

Figure 10. Specificity of α-*Li*mFRD and α-*Li*NDH2 antibodies. Western blot analysis upon SDS-PAGE using α-*Li*mFRD and α-*Li*NDH2 antibodies. PurifiedHis_6*Li*mFRD and His_6*Li*NDH2 proteins were used as positive controls. Total protein extracts from *L. infantum* wt, OE_*Li*mFRD-cMyc and OE_*Li*NDH2-cMyc strains grown at early (EL) and late logarithmic phases (LL) were analyzed. The same number of parasites ($5x10^6$) was loaded in each lane.

The analysis of figure 10 shows that α-*Li*mFRD and α-*Li*NDH2 recognize the respective recombinant protein, showing thus, its specificity. Moreover, both antibodies recognize proteins in the different growth stages of the parasite, confirming that both proteins are expressed in these phases (early logarithmic and late logarithmic) in wild type, OE_*Li*mFRD-cMyc and OE_*Li*NDH2-cMyc strains. In figure 10A, a band of approximately 129.7 kDa corresponding to the molecular weight of the *Li*mFRD is detected in wild type and an increased expression is observed in the overexpressing strain. In figure 10B a band is recognized corresponding to the expression of *Li*NDH2, at 57.5 kDa, and an increased expression is detected in the respective overexpressing strain.

With this new tool, we can now characterize various aspects of *Li*mFRD and *Li*NDH2 proteins. We began by addressing the expression of either protein in amastigotes through western blot analysis of protein extracts from wild type (figure 11).

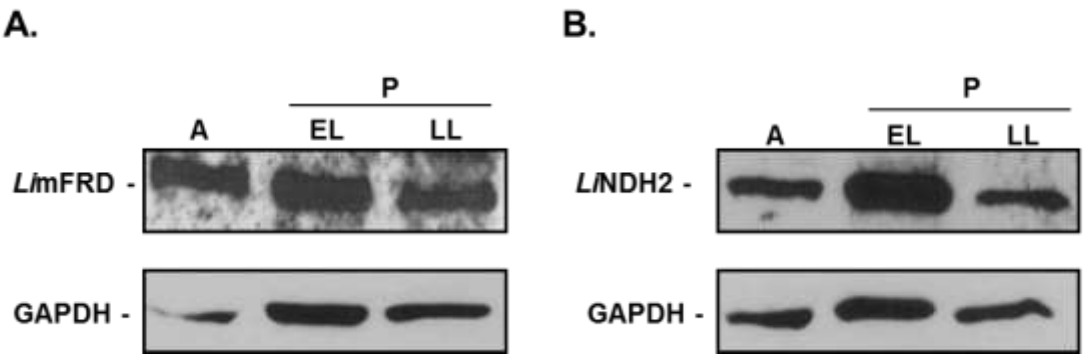

Figure 11. *Li*mFRD and *Li*NDH2 are expressed in axenic amastigotes of *L. infantum.* Total protein extracts from wt promastigotes (P) grown at early (EL) and late logarithmic (LL) phases and amastigotes (A) grown at logarithmic phase were analyzed by western blotting with antisera against *Li*mFRD (A) or *Li*NDH2 (B). The same number of parasites ($5x10^6$) was loaded in each lane**.**

Western blot analysis shows the expression of both proteins, *Li*mFRD and *Li*NDH2, in amastigotes (figure 11). Our results reveal that both proteins are expressed in axenic amastigote forms with the expected molecular weights - 129.7 kDa for *Li*mFRD and 57.5 kDa for *Li*NDH2- indicating that no alterations in the proteins occur in the different forms of the parasite. No significant differences were observed in *Li*mFRD expression between amastigotes and promastigotes, although early log promastigotes seem to have a slight increase in expression of *Li*NDH2.

The expression of cMyc tagged *Li*mFRD in the OE_*Li*mFRD-cMyc strain was evaluated by western blotting analysis upon growth with increasing concentrations of G418. As we can see in figure 12, increased G418 concentration does not led to a corresponding increase in tagged-*Li*mFRD protein expression and thus, the lowest concentration of G418 was used henceforward. The same result was verified for tagged-*Li*NDH2 (data not shown).

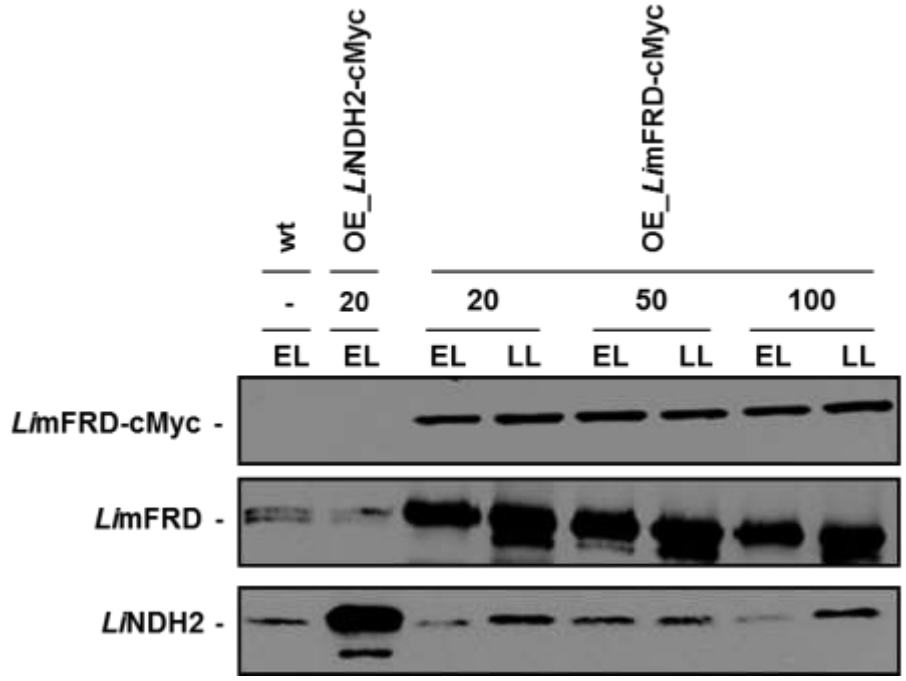

Figure 12. Increasing G418 concentrations does not affect expression of tagged-*Li*mFRD. Expression of *Li*mFRD in the OE_*Li*mFRD-cMyc was evaluated by western blotting with antisera against cMyc, *Li*mFRD and *Li*NDH2. Wild type and OE_*Li*NDH2-cMyc promastigotes strains were grown at early (EL) logarithmic phase and OE_*Li*mFRD-cMyc were grown at early (EL) and late (LL) logarithmic phases with increasing concentrations of G418. The same number of parasites ($5x10^6$) was loaded in each lane.

4.3 Localization of *Li*mFRD and *Li*NDH2 proteins in *L. infantum*

To determine the subcellular localization of *L. infantum* *Li*mFRD and *Li*NDH2 proteins, digitonin assay, immunofluorescence and carbonate extraction assays were carried out.

4.3.1 Digitonin/proteinase K assay

Wild type parasites were used in order to determine the subcellular localization of *Li*mFRD and *Li*NDH2 endogenous protein. Based on the differential composition of the cellular membranes, the subcellular compartments are differentially permeabilized by the non-ionic detergent digitonin, with glycosomes and mitochondrial membranes being more resistant to this detergent. After solubilization with digitonin, proteinase K was added to degrade accessible proteins. The patterns of extraction and degradation of *Li*mFRD and *Li*NDH2 were compared with the following markers: mTPx, *Li*TryS and arginase. The mitochondrial peroxiredoxin (mTPx) (64) was used as a mitochondrial marker, trypanothione synthetase (*Li*TryS) (65) as a cytosolic protein and arginase (66) as a glycosomal marker.

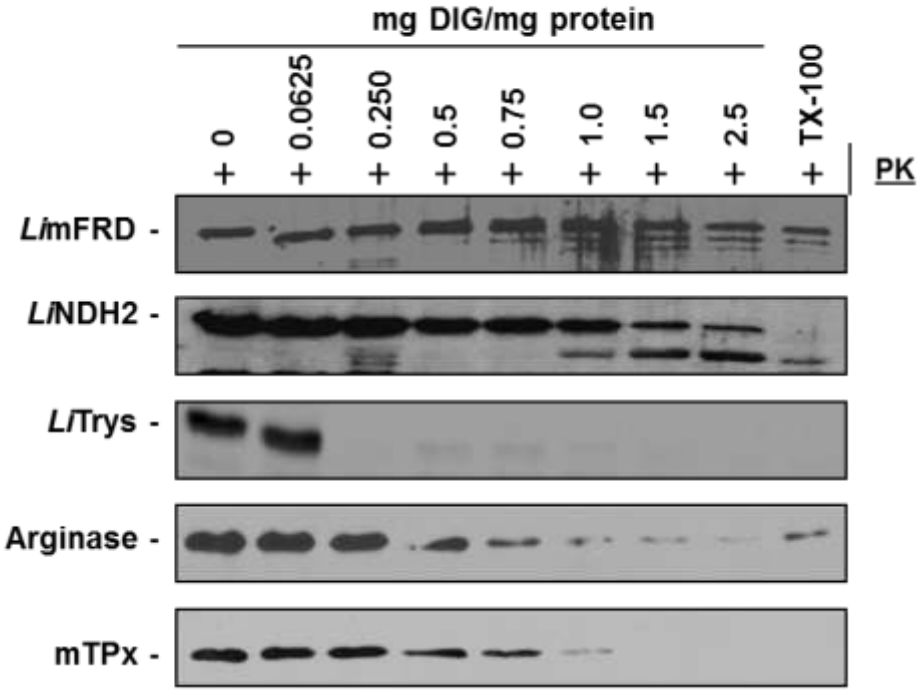

Figure 13. Protease accessibility upon digitonin solubilization of wt parasite membranes. Protein samples resulting from the permeabilization of wt promastigotes with increasing concentrations of digitonin in the presence of proteinase K were analyzed by western blotting with antibodies against the indicated proteins. Arginase, mTPx and *Li*TryS were used as controls.

Results in figure 13 show that *Li*NDH2 protein is digested at approximately 1 mg DIG/mg protein and the same pattern is observed for the mitochondrial marker mTPx and thus, we concluded that *Li*NDH2 is a mitochondrial protein (figure 13), as expected. On the other hand, *Li*mFRD protein is insensitive to proteinase K degradation and hence it is not possible to conclude about its subcellular localization by this procedure. To confirm that *Li*mFRD is indeed resistant to proteinase K, we tested its sensitivity to protease degradation in different assay conditions (figure 14). We used different detergents to solubilize wt parasites (DIG, Nonidet P-40, SDS or Triton X-100) and different proteases (PK and trypsin). Figure 14 shows that PK only digested *Li*mFRD when in the presence of SDS, thus, when *Li*mFRD is denatured and that in all the other conditions *Li*mFRD is resistant to degradation as confirmed by comparison with the control *Li*NDH2. Moreover, even in the presence of SDS *Li*mFRD is resistant to trypsin degradation.

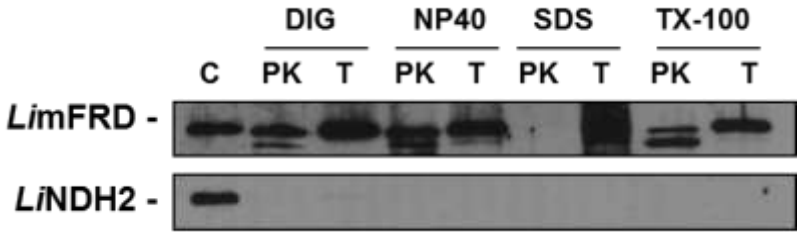

Figure 14. *Li*mFRD is resistant to proteases degradation. Wild type promastigotes were solubilized with 1% of digitonin (DIG), Nonidet P-40 (NP40), sodium dodecyl sulphate (SDS) or Triton X-100 (TX-100) detergents in the presence of either proteinase K (PK) or trypsin (T). The resulting samples were analyzed by western blotting with antiserum against *Li*mFRD and *Li*NDH2.

Due to the experimental limitation referred above, we decided to use OE_*Li*mFRD-cMyc parasites in order to determine the subcellular localization of cMyc tagged *Li*mFRD. Although we knew that the endogenous protein is resistant to degradation by PK, the behavior of the overexpressed protein was not known.

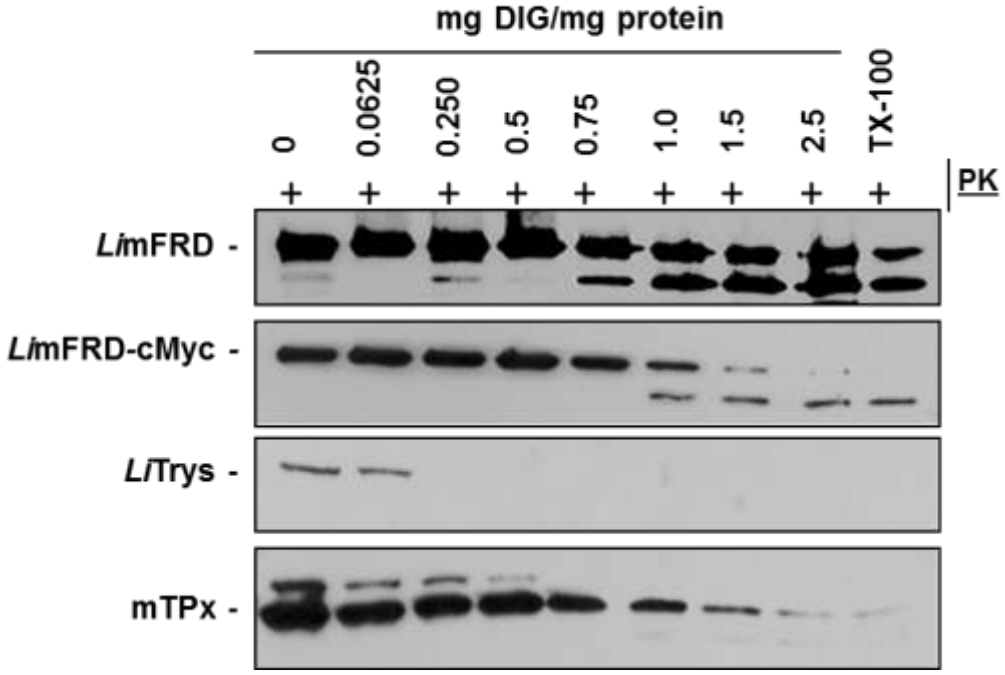

Figure 15. Protease accessibility upon digitonin solubilization of OE_*Li*mFRD-cMyc parasite membranes. Protein samples resulting from the permeabilization of OE_*Li*mFRD-cMyc promastigotes with increasing concentrations of digitonin in the presence of proteinase K were analyzed by western blotting with antibodies against the indicated proteins. mTPx and *Li*TryS were used as controls.

Curiously, the results of protease accessibility (figure 15) show that *Li*mFRD-cMyc was digested by PK at approximately 1 mg DIG/mg protein in a pattern similar to that observed for the mitochondrial marker mTPx, leading us to concluded that *Li*mFRD-cMyc protein is located in the mitochondria. However, the endogenous protein

maintains its resistance to degradation as previously observed for the wild type (figure 13). The different behavior of the endogenous and tagged *Li*mFRD proteins to PK suggests that, although both can be localized in the mitochondrion, differences in the conformation or post-translational modification should exist between them.

4.3.2 Immunofluorescence

To confirm the subcellular localization of *Li*NDH2 and *Li*mFRD proteins in *L. infantum*, promastigotes cultured during 3 days were analyzed by indirect immunofluorescence. DAPI was used to stain the nucleus and kinetoplast (blue), an antibody against mTPx was used to detect the mitochondrion (red), and antibodies against the *Li*NDH2, the *Li*mFRD and the *Li*mFRD-cMyc to stain *Li*NDH2, *Li*mFRD and *Li*mFRD-cMyc proteins (green).

4.3.2.1 Localization of *Li*NDH2

OE_*Li*NDH2-cMyc *L. infantum* promastigotes were labeled with α-*LiN*DH2 and α-mTPx antibodies and analyzed by immunofluorescence. As shown in figure 16, the *Li*NDH2 signal completely overlaps with that of mTPx, confirming that *Li*NDH2 is a mitochondrial protein, in accordance with the results obtained in digitonin/proteinase K assays.

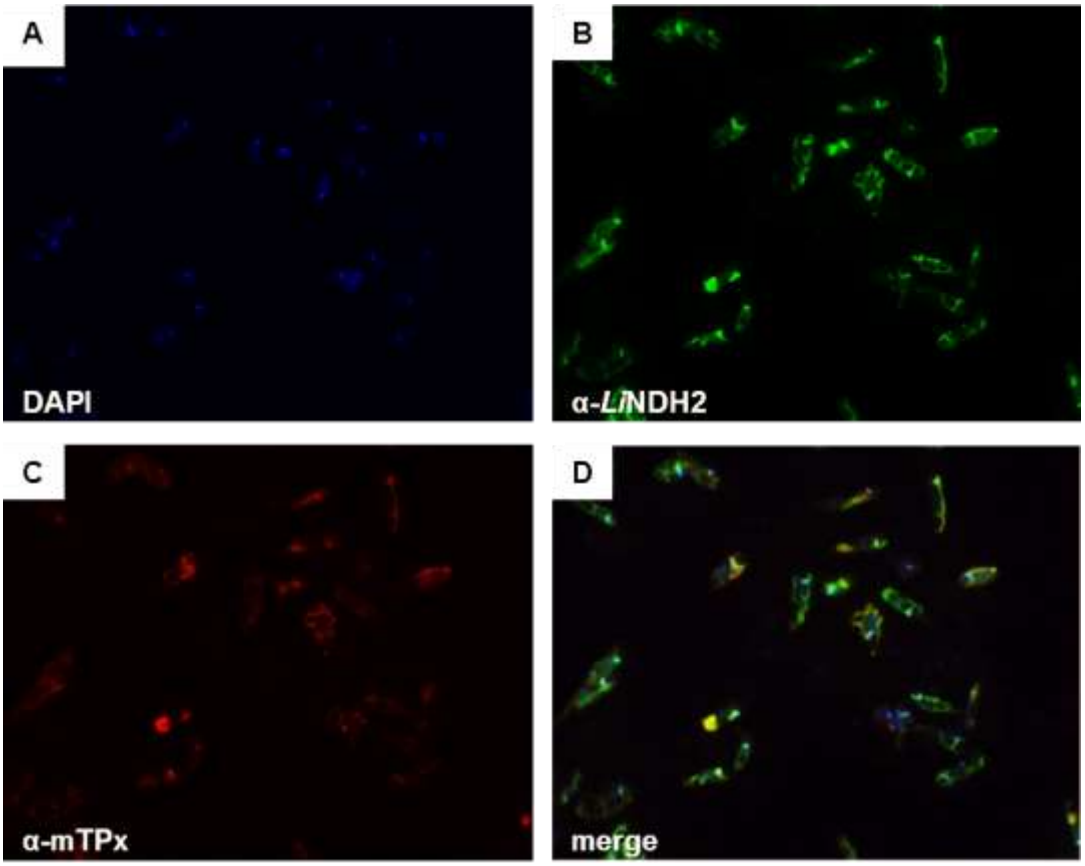

Figure 16. Localization of *Li*NDH2. OE_*Li*NDH2-cMyc promastigotes were labeled with DAPI (A), α-*Li*NDH2 (B) and α-mTPx (C). The merged images are shown in panel (D). The cells were visualized in a Zeiss Axio Imager Z1 microscope.

4.3.2.2 Localization of *Li*mFRD

In order to investigate the subcellular localization of *Li*mFRD we performed immunofluorescence assays using the OE_*Li*mFRD-cMyc promastigotes labeled with α-*Li*mFRD and α-mTPx. The signal obtained with α-*Li*mFRD is faint and does not totally overlap with that observed for the mitochondrial marker, α-mTPx (figure 17), rendering the precise *Li*mFRD localization unclear. This faint staining may be due to the fact of the α-*Li*mFRD antibody has been produced against the denatured protein and thus may not recognize *Li*mFRD in immunofluorescence assays. In order to overcome this possible problem, we used α-cMyc to recognize the tagged *Li*mFRD overexpressed protein (figure 18).

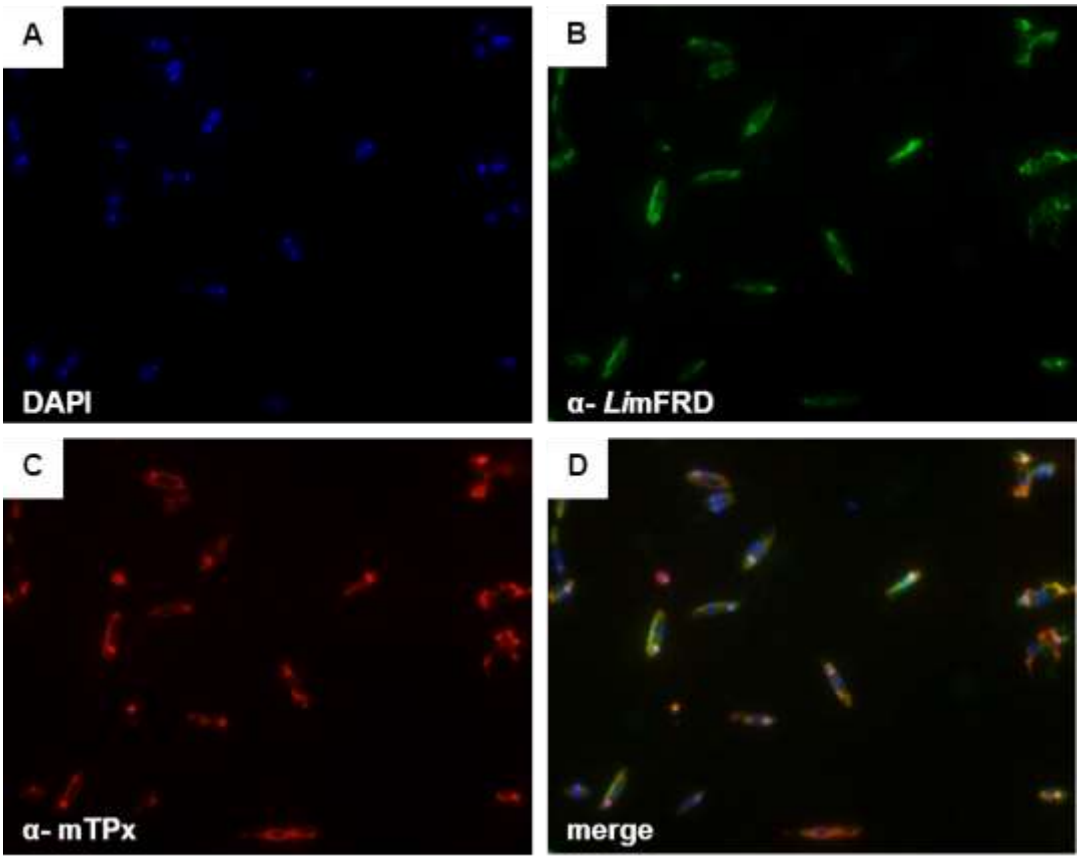

Figure 17. Localization of *Lim*FRD. OE_LimFRD-cMyc promastigotes were labeled with DAPI (A), α-LimFRD (B) and α-mTPx (C). The merged images are shown in panel (D). The cells were visualized in a Zeiss Axio Imager Z1 microscope.

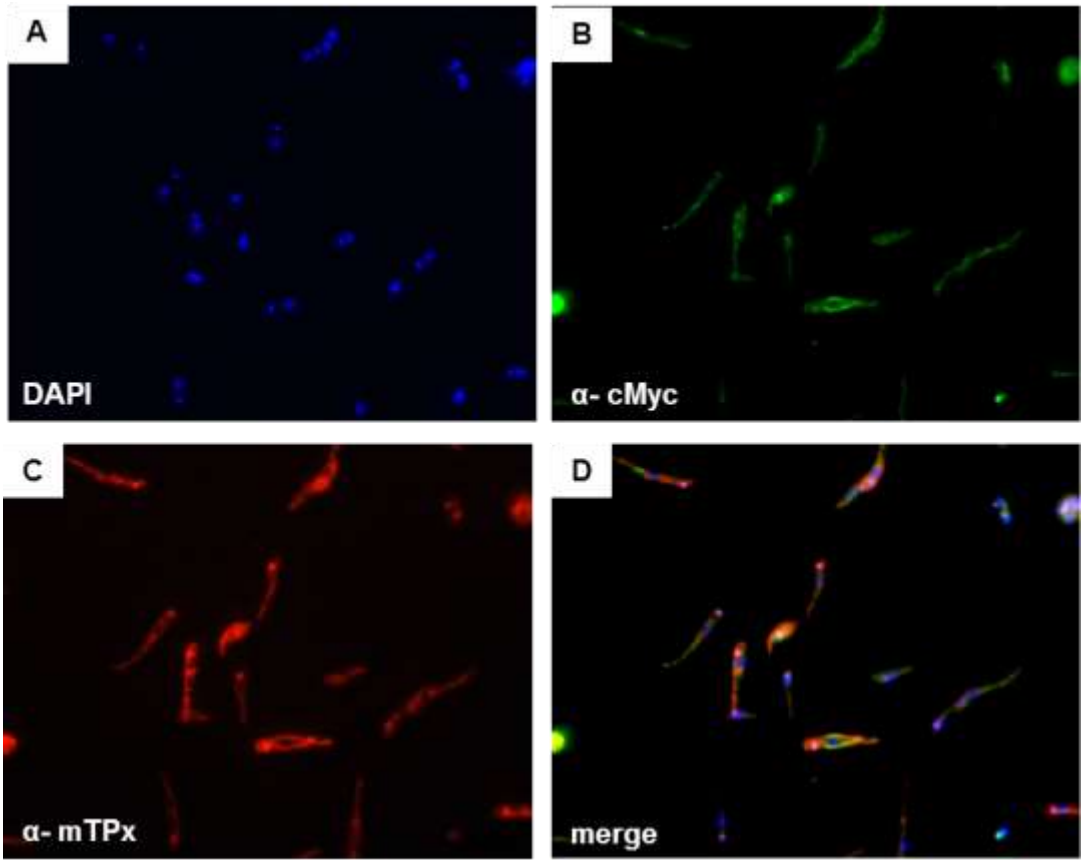

Figure 18. Localization of cMyc tagged-*Li*mFRD. OE_*Li*mFRD-cMyc promastigotes were labeled with DAPI (A), α-cMyc (B) and α-mTPx (C). The merged images are shown in panel (D). The cells were visualized a Zeiss Axio Imager Z1 microscope.

As can be observed in figure 18, *Li*mFRD-cMyc protein is detected in the mitochondrion of most parasites but its distribution does not entirely co-localize with mTPx staining. We confirmed that this protein was not localized in glycosomes, since no immunostaining overlap was observed between *Li*mFRD-cMyc and a glycosomal marker in an immunofluorescence assay (data no shown). Our results indicate that *Li*mFRD-cMyc localizes to the mitochondrion.

4.3.3 *Li*mFRD is a soluble protein and *Li*NDH2 is associated with the mitochondrial membrane

To investigate whether *Li*mFRD and *Li*NDH2 are associated with the mitochondrial membranes or if they are instead soluble proteins, alkaline carbonate extraction was performed. It was previously described that in some trypanosomatids mFRD is a hydrophilic protein associated with the mitochondrial membrane (62). Moreover, *Li*NDH2 orthologous have being described as either integral membrane

proteins (67) or extrinsic membrane proteins (51). Wild type and OE_*Li*mFRD-cMyc promastigotes were used for carbonate extraction.

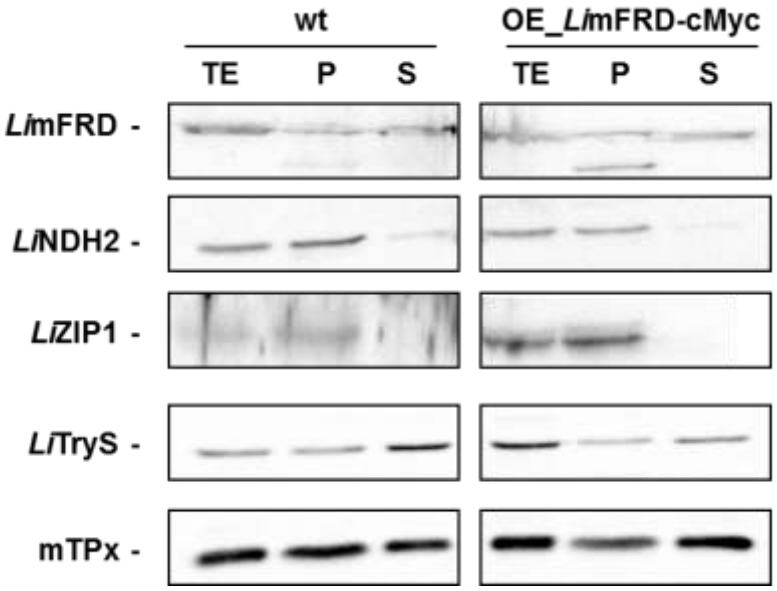

Figure 19. *Li*mFRD is soluble and *Li*NDH2 is found associated with the membrane. Wild type and OE_*Li*mFRD-cMyc promastigotes were extracted with 0.1M Na_2CO_3 and total protein extracts (TE), supernatants (S) and membrane pellets (P) resulting from fractionation were analyzed by western blotting using antibodies against the indicated proteins.

Figure 19 shows that *Li*mFRD is distributed between the pellet and the supernatant in both the wt and the OE_*Li*mFRD-cMyc strains. This result indicates that *Li*mFRD, although a hydrophilic protein, seems to have an interaction with the membrane. However, looking carefully to the soluble controls, mTPx and *Li*TryS, we notice that both proteins are distributed between the pellet and the supernatant fractions. A possible explanation for this observation (given that mTPx and *Li*TryS are known soluble proteins) is contamination of the pellet fractions with intact parasites. Considering these results, we may conclude that both *Li*mFRD and *Li*mFRD-cMyc are soluble proteins. On the other side, *Li*NDH2 is mainly present in the pellet fraction, indicating that this protein is associated with the mitochondrial membrane. *Li*ZIP1 is a transmembrane transporter that is detected only in the pellet fraction, as expected.

4.4 Enzymatic assays in bacteria and parasite membranes

Enzymatic assays were performed attempting to determine the kinetic parameters of *Li*mFRD and *Li*NDH2 enzymes, in order to characterize them. Initially, measurements of NADH-Q_1 and NADH-fumarate reductase activities were performed

in bacterial membranes from non-induced controls and induced overexpressing strains. Yet, no differences between the analyzed strains were detected. This suggests that either the fusion proteins were not active in the bacterial membranes or they have aggregated during membrane preparation, given that alterations in membrane properties were verified.

Alternatively, we attempted to measure the same NADH-Q_1 and NADH-fumarate reductase activities using parasite membranes from wt, OE_*Li*mFRD-cMyc and OE_*Li*NDH2-cMyc strains. Nonetheless, once again, the same difficulty was observed since, although we could measure NADH consumption, alterations between wt and the overexpression strains were not observed. Taking these results into account, respiratory assays were performed to try to overcome this drawback. With these assays we wanted to characterize the differences between wt, OE_*Li*mFRD-cMyc and OE_*Li*NDH2-cMyc strains in order to ascertain the function of *Li*mFRD and *Li*NDH2 in the respiratory chain of *L. infantum*.

4.5 Oxygen consumption in *L. infantum*

In order to study the effects of overexpressing *Li*mFRD and *Li*NDH2 on the respiration process we measured oxygen consumption in *L. infantum* with an oxygen electrode. Moreover, we evaluate the effects of respiratory chain inhibitors namely, rotenone, TTFA and KCN as inhibitors of complex I, II and IV, respectively. In figure 20, we can observe an example of the action of the inhibitors in oxygen consumption by intact *L. infantum* parasites, obtained from O2view software.

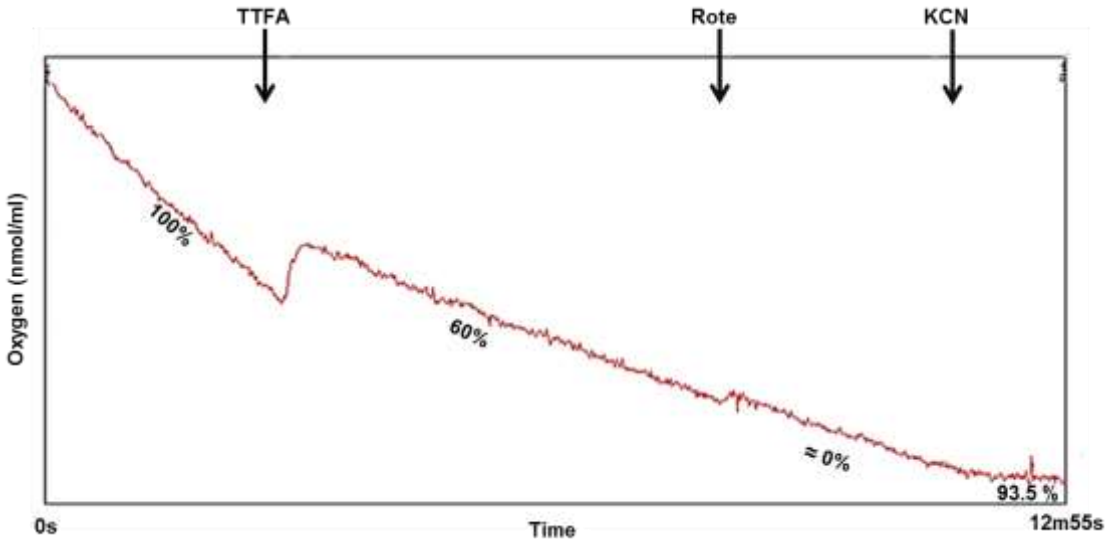

Figure 20. OE_*Li*NDH2-cMyc promastigotes respiration. Representative assay of basal oxygen consumption by promastigotes upon sequential inhibition with 2 mM TTFA, 60 µM rotenone and 1mM KCN to the reaction medium. Results were acquired with O2view software. Percentages of inhibition by TTFA and KCN were determined relatively to the initial oxygen consumption rate. Rotenone inhibition was calculated relatively to oxygen consumption upon TTFA inhibition.

As we can see in the figure above, addition of inhibitors leads to a decrease in the slope of the line, which reflects a decrease in oxygen consumption. After the addition of TTFA a slope decrease is observed, meaning that complex II is involved in O_2 consumption. Moreover, when rotenone is added the inhibition of oxygen consumption is not significant indicating a negligible contribution of complex I to respiration. On the other hand, reduction of O_2 is mainly performed by complex IV, since KCN almost completely inhibits respiration (figure 20).

In figure 21, basal oxygen consumption and oxygen consumption upon inhibition by TTFA and KCN were determined for intact *L. infantum* promastigotes of the wt, OE_*Li*NDH2-cMyc and OE_*Li*mFRD-cMyc strains, grown to the logarithmic phase. The values of basal oxygen consumption (nmol $O_2.min^{-1}.mg^{-1}$) and the percentages of inhibition by 2 mM TTFA and 1 mM KCN, are summarized in table 6.

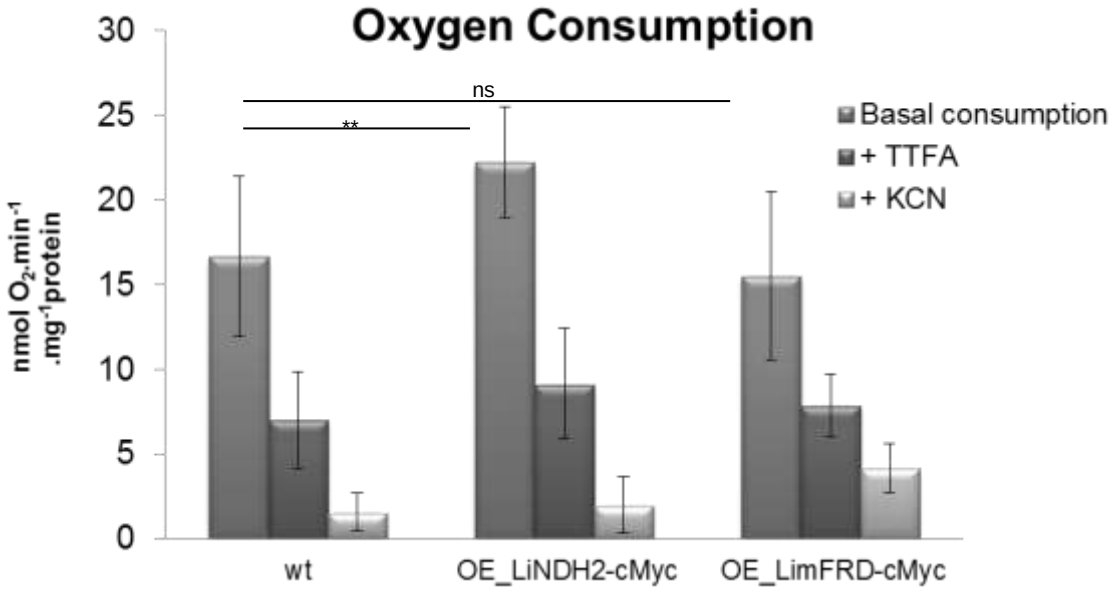

Figure 21. Oxygen consumption by *L. infantum* promastigotes. Basal oxygen consumption and oxygen consumption upon TTFA and KCN inhibition of the wt, OE_*Li*NDH2-cMyc and OE_*Li*mFRD-cMyc parasites were measured polarographically at RT with a Clark-type oxygen electrode. Results were evaluated with O2view software. Errors bars represent standard deviation. ns- non significant, **P<0.01 as calculated by t-test in Graph Pad Prism.

Table 6. Basal oxygen consumption in *L. infantum* promastigotes. Basal oxygen consumption of the wt, OE_*Li*NDH2-cMyc and OE_*Li*mFRD-cMyc parasites grown for 3 days was determined. TTFA and KCN inhibition is shown as percentage of the basal rate. Data are expressed as average ± SD of n independent experiments.

Strains	Basal O_2 consumption (nmol $O_2.min^{-1}.mg^{-1}$)	TTFA inhibition (%)	KCN inhibition (%)
WT	16.66 ± 4.71 (n= 11)	58.00	90.70
OE_*Li*NDH2-cMyc	22.23 ± 3.27 (n= 6)	58.90	91.10
OE_*L*imFRD-cMyc	15.53 ± 4.99 (n=8)	49.30	73.30

The results show that the OE_*Li*NDH2-cMyc strain displays the highest basal oxygen consumption reaching 22.23 ± 3.27 nmol $O_2.min^{-1}.mg^{-1}$protein followed by wt (16.66 ± 4.71 nmol $O_2.min^{-1}.mg^{-1}$protein) and the OE_*Li*mFRD-cMyc (15,53 ± 4,99 nmol nmol $O_2.min^{-1}.mg^{-1}$protein), as illustrated in figure 21 and table 6. These results suggest that overexpression of these NADH oxidizing enzymes has some impact on mitochondrial respiration. The susceptibility of the different *L. infantum* promastigotes

to mitochondrial respiratory chain inhibitors was also evaluated. Rotenone, an inhibitor of complex I does not affect oxygen consumption, suggesting that complex I is not involved in basal oxygen consumption under the tested conditions (data not shown). Inhibition with TTFA has a similar behavior in wt and OE_*Li*NDH2-cMyc and a slightly minor effect in OE_*Li*mFRD-cMyc respiration (Table 6). When we used KCN the inhibitory effect verified was approximately the same for wt and OE_*Li*NDH2-cMyc (90-91% inhibition) and, once again, OE_*Li*mFRD-cMyc was less inhibited (74%).

The oxygen consumption inhibited by TTFA (Figure 22), a complex II inhibitor, can be considered as the respiratory rate contributed by complex II activity (basal oxygen consumption-TTFA).

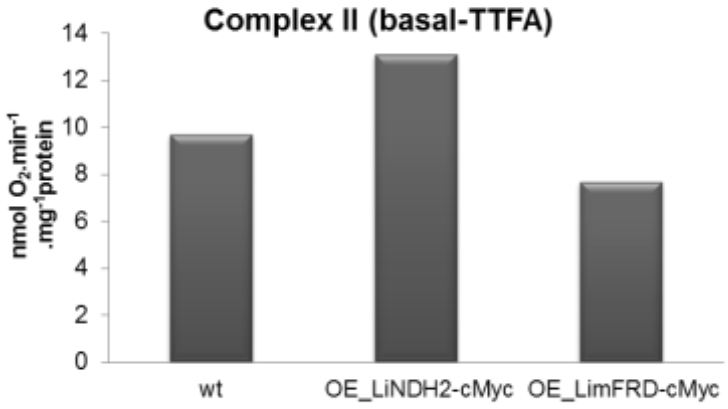

Figure 22. Oxygen consumption inhibited by TTFA. Oxygen consumption from wt, OE_*Li*NDH2-cMyc and OE_*Li*mFRD-cMyc parasites grown during 3 days was measured polarographically at RT with a Clark-type oxygen electrode and results were evaluated with O2view software.

As seen in figure 22 and table 7 the major oxygen consumption dependent on complex II activity is achieved by OE_*Li*NDH2-cMyc and wt (13.10 ± 3.26 and 9.67 ± 2.85 nmol O_2.min^{-1}.mg^{-1}protein, respectively), while the lowest was verified in OE_*Li*mFRD-cMyc being 7.66 ± 1.83 nmol O_2.min^{-1}.mg^{-1} protein, suggesting that this complex is less involved in respiration in this strain. Moreover, overexpression of *Li*NDH2 leads to an increase in basal oxygen consumption accompanied by an increase contribution of complex II.

Table 7. Effect of the respiratory chain inhibitors TTFA and KCN in oxygen consumption. Data are expressed as average ± SD of n independent experiments. Oxygen consumption was measured polarographically at RT with a Clark-type oxygen electrode and results were evaluated with O2view software.

Strains	Basal O_2 consumption	Basal – TTFA	TTFA – KCN
	($nmol\ O_2.min^{-1}.mg^{-1}$)		
WT	16.66 ± 4.71 (n=11)	9.67 (n=7)	5.44 (n=6)
OE_*Li*NDH2-cMyc	22.23 ± 3.27 (n=6)	13.10 (n=5)	7.15 (n=6)
OE_*Li*mFRD-cMyc	15.53 ± 4.99 (n=8)	7.66 (n=6)	3.74 (n=7)

Figure 23 illustrates the oxygen consumption attributed to enzymes able to feed electrons into quinone of the ERC, namely complex I, *Li*NDH2, G3PDH and probably other uncharacterized reductases, not sensitive to complex II inhibitors. This respiratory rate is determined as the KCN sensitive and TTFA resistant oxygen consumption (TTFA-KCN). The highest rate is observed for OE_*Li*NDH2-cMyc (7.15 ± 1.65 nmol $O_2.min^{-1}.mg^{-1}$), suggesting that it is the result of overexpressing *Li*NDH2. In wt and OE_*Li*mFRD-cMyc the TTFA-KCN rates were smaller (5.44 ± 1.12 and 3.74 ± 1.46 nmol $O_2.min^{-1}.mg^{-1}$, respectively) than in OE_*Li*NDH2-cMyc. The low rate observed in OE_*Li*mFRD-cMyc is probably due to a decreased contribution of *Li*NDH2 in oxygen consumption resulting from the overexpression of *Li*mFRD, an enzyme involved in NADH oxidation as *Li*NDH2 but not in a KCN sensitive pathway.

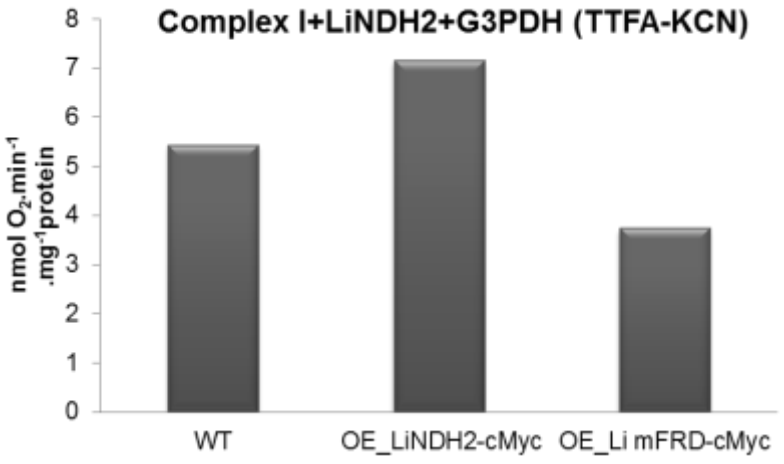

Figure 23. Oxygen consumption sensitive to KCN and resistant to TTFA. Oxygen consumption from wt, OE_*Li*NDH2-cMyc and OE_*Li*mFRD-cMyc parasites grown for 3 days was measured polarographically at RT with a Clark-type oxygen electrode and results were evaluated with O2view software.

4.6 *L. infantum* sensitivity to OXPHOS inhibitors

To test the sensitivity of *L. infantum* promastigotes growth to OXPHOS inhibitors we used wt, OE-*Li*NDH2_cMyc and OE-*Li*mFRD_cMyc strains according to materials and methods and performed a comparative analysis.

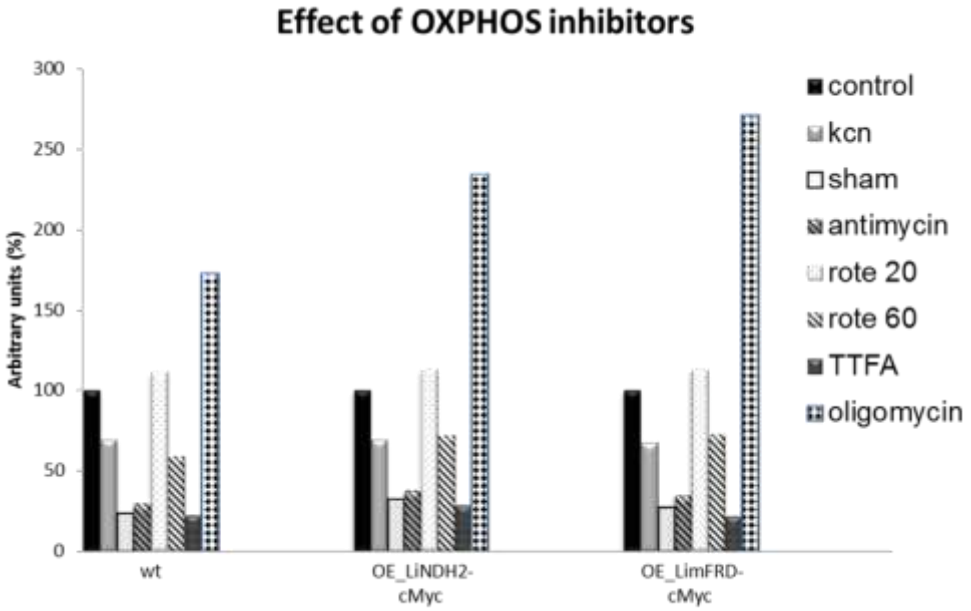

Figure 24. Inhibition of proliferation of *L. infantum* promastigotes by inhibitors of the OXPHOS. Promastigotes were cultured during three days in the presence of inhibitors (1 mM for KCN, 20 and 60 µM for rotenone, 2 mM for TTFA, 2 $\mu g.ml^{-1}$ for antimycin A, 2 $\mu g.ml^{-1}$ for oligomycin and 5 mM for SHAM). The final growth was evaluated by measuring OD_{600nm} using a spectrophotometer.

As we can see, in the presence of KCN or 60 µM rotenone, *L. infantum* growth was inhibited by about 40% in comparison to the controls without inhibitors. A similar pattern of growth inhibition was observed for SHAM, antimycin A or TTFA, which resulted in approximately 80% growth inhibition. On the other side, oligomycin or low rotenone concentrations (20 µM) did not inhibit parasite growth with oligomycin even promoting parasite proliferation (figure 24). This increase in proliferation is more pronounced in OE_*Li*mFRD-cMyc strain. The pattern of growth inhibition by OXPHOS drugs is similar in all the strains analyzed with only a minor difference upon oligomycin addition.

Discussion

Mitochondrial fumarate reductase (mFRD) and alternative NADH dehydrogenase (NDH2) are proteins involved in mitochondrial metabolism through NADH oxidation. mFRD was identified in prokaryote and eukaryote organisms. This protein is usually a multi-subunit complex able to use reduced quinone as an electron donor that in eukaryotes is associated to the mitochondrial membrane. In trypanosomatids, mFRD is a single polypeptide enzyme that uses NADH to reduce fumarate and thus is accountable for matrix NADH oxidation. NDH2 was identified in several fungi, plants and primitive eukaryotic cells and can be localized in the external or internal face of the inner mitochondrial membrane. Knowledge of the exact localization of NDH2 in the mitochondria is important to understand if this enzyme oxidizes NADH resulting from catabolic processes that occur in the mitochondria or NADH produced in the cytosol. In the first case the enzyme is located at the inner face of the inner membrane of the organelle and can perform the same role as complex I with the exception that this last one also has proton translocation activity. In the second case, the enzyme is located in the outer face of the inner membrane and does not replace complex I, being responsible for the regeneration of cytosolic NAD^+. These enzymes are absent from mammalian cells, and this fact makes them potential drug targets to control diseases caused by trypanosomatids (16,41).

To understand the role of *Li*mFRD and *Li*NDH2 within the mitochondrial respiratory chain we set out to identify their subcellular localization and to characterize the overexpressing strains, OE_*Li*mFRD-cMyc and OE_*Li*NDH2-cMyc. For this purpose, we studied the expression and localization of the proteins in *L. infantum* parasites, and analyzed changes in oxygen consumption and parasite growth mediated by known oxidative phosphorylation inhibitors.

Regarding the expression of *Li*mFRD and *Li*NDH2 proteins in *L. infantum*, we conclude that both proteins are expressed in different forms of the parasite (promastigote and amastigote) and in different growth stages (early log and late log), suggesting that no alterations in the proteins occur in the different forms of the parasite. Furthermore, expression of *Li*NDH2 and *Li*mFRD in amastigotes validates the potential value of these proteins as drug targets.

Both enzymes are predicted as mitochondrial proteins by *in silico* analysis. Subcellular localization of the proteins was determined with several biochemical assays confirming that both proteins are located in the mitochondria. *Li*mFRD is a soluble enzyme as described for its orthologous in *T. brucei* (22). *Li*NDH2 is associated to the mitochondrial inner membrane although its exact localization, with catalytic sites facing

the external intermembrane space or the internal mitochondrial matrix of *L. infantum* parasites, requiring further investigation. Given that the internal NDH2 enzyme of *S. cerevisiae* was described as a monotopic protein (34), we speculate that *Li*NDH2 may also be an integral membrane protein that interacts only to one side of the inner mitochondrial membrane.

The kinetic parameters of *Li*mFRD and *Li*NDH2 enzymes were not determined due to experimental difficulties. Overexpression of both proteins in either *E. coli* or *L. infantum* did not result in differences in their specific biochemical activities when compared to the control, preventing us to biochemically characterize any of the proteins. Though the experimental procedures involved the preparation of membranes, a harsh task, we were able to measure NADH oxidation either using Q_1 or fumarate as electron acceptors. Yet, no specific inhibitor for any of the enzymes is available what makes it difficult to identify the NADH oxidation activity performed by *Li*NDH2 or *Li*mFRD, as no increase in the respective activities was observed upon overexpression.

To circumvent this difficulty, oxygen consumption assays were performed comparing overexpressing strains with the wild type. Our data shows that the basal oxygen consumption is higher upon *Li*NDH2 overexpression, in the OE_*Li*NDH2-cMyc, than in wt and OE_*Li*mFRD-cMyc although in all the strains complex II, III and IV are involved in respiration. The higher respiration in OE_*Li*NDH2-cMyc is associated with an increase in complex II activity and an increase in the activity of enzymes that feed electrons into the first entry point of the respiratory chain (including NDH2, G3PDH and complex I). Since inhibition of oxygen consumption by rotenone, a specific inhibitor of complex I, is very low we assumed that either complex I is not being expressed under the experimental conditions used or rotenone is not able to inhibit the *L. infantum* enzyme. This low inhibition was observed for all the tested strains and previously described as a characteristic of several trypanosomatids respiration (40,62). Moreover, it was shown that knocking down NDH2 in procyclic *T. brucei* results in increased G3PDH activity (61,68). Hypothesizing that the reverse situation may occur, we would expect that overexpression of *Li*NDH2 in the OE_*Li*NDH2-cMyc strain decreases G3PDH activity and thus, *Li*NDH2 is the main enzyme feeding electrons into the first entry point of the respiratory chain (oxygen consumption inhibited by KCN and resistant to TTFA, Figure 23). This interrelationship between NDH2 and G3PDH was previously described also for yeast where it was shown that both external NADH dehydrogenases and G3PDH compete for electron supply to the respiratory chain (69,70).

Overexpression of *Li*mFRD leads to a decreased rate of oxygen consumption with an increased resistance to the complex IV inhibitor KCN (Figure 21). This lower sensitivity of OE_*Li*mFRD-cMyc to KCN suggests that oxygen consumption is not totally used by the respiratory chain being probably associated with ROS production. The *Li*mFRD enzyme produces succinate via fumarate oxidation, implying that, upon overexpression and if fumarate is present in limiting amounts, ROS can be produced. Previous findings in *T. brucei* indicate that, in the absence of fumarate, FRD becomes an intracellular source of reactive oxygen species such as superoxide anion and hydrogen peroxide (32).

The increase in complex II activity observed in OE_*Li*NDH2-cMyc may be associated with an increase in Krebs cycle activity as described before for procyclic *T. brucei* (71). The diminished basal oxygen consumption upon *Li*mFRD overexpression can result from the decreased activity of NDH2, since both enzymes oxidize the NADH substrate. Consequently, fewer electrons from NADH enter the respiratory chain while succinate production increases as may increase the electron flux through complex II. Because the activity of complex II in the OE_*Li*mFRD-cMyc strain is even lower than in the wild type we speculate that succinate is probably being excreted.

Based on the oxygen consumption results, the effects of OXPHOS inhibitors in *L. infantum* promastigotes growth were evaluated. As referred above, complex I appears to be absent in *L. infantum* promastigotes (Figure 20). However, elevated rotenone concentrations (60 µM) inhibited parasite growth by around 40% while smaller rotenone concentrations have no effect on growth. Previous studies showed that lower concentrations of rotenone were sufficient for growth inhibition of other *Leishmania* spp (14). Our results suggest that inhibition of *L. Infantum* growth by rotenone is probably due to an unspecific effect of the drug. In fact, it was previously described that high amounts of rotenone can inhibit FRD (62).

Growth inhibition using KCN is expected to be close to total, as complex IV seems to be the only respiratory enzyme reducing oxygen. Surprisingly, only about 40% growth inhibition was observed for all the 3 strains in the presence of KCN (Figure 24), indicating that either the amount of inhibitor is not sufficient for complete inhibition of growth or an alternative pathway exists to reduce oxygen, which is induced in the presence of KCN. In fact, it is known for a long time that fungi, plants and protozoa possess an alternative oxidase, able to replace complex III and IV function. This alternative oxidase is present in *T. brucei* procyclic and bloodstream forms and is inhibited by SHAM (38), but was not described for *Leishmania* spp. We looked for such an enzyme through genome mining in *L. infantum* using the sequence of AOX from *T.*

brucei. A gene encoding a putative alternative oxidase was identified in the genome of *L. infantum* (LinJ36.4980) and it is conserved in many other trypanosomatids including *T. brucei* (where two alternative oxidases exist). The protein encoded by the referred gene was identified in the mitochondrial proteome of *T. brucei* (72). Surprisingly, SHAM inhibits *L. infantum* growth almost completely as observed for antimycin A and TTFA. However, a huge concentration of SHAM (5 mM) was tested what could result in unspecific effects. Using lower concentrations of inhibitor a less drastic effect on parasite growth was observed (data not shown).

The lethal effect of TTFA (inhibitor of complex II) and antimycin A (inhibitor of complex III) suggests that both complex II and complex III are essential for *L. infantum* promastigote survival in the tested conditions in the presence of glucose. In procyclic forms of *T. brucei*, complex II was shown to be essential for parasites survival only in glucose-depleted conditions (71). The great inhibition by the complex III inhibitor emphasizes the importance of this enzyme for *L. infantum*, whereas no need for this complex is described for other trypanosomatids (35). In fact, the result obtained with antimycin A and KCN is difficult to reconcile, as both inhibitors should have the same effect on growth. A possible explanation for this discrepancy is that only inhibition by KCN (complex IV) induces the hypothetical alternative oxidase. Another puzzling observation was the effect of the inhibitor of ATP synthase, oligomycin, which instead of reducing growth by decreasing ATP production, leads to increased proliferation of the parasites. This indicates that ATP production can occur by pathways other than OXPHOS, probably glycolysis. Moreover, the increased proliferation can be due to a transition for a more glycolytic metabolism instead of the predominantly oxidative phosphorylation. This recalls the situation of cancer cells where the increased glycolytic flux, associated with a decreased oxidative metabolism, results in cell proliferation (73).

Future work

The energetic metabolism of *Leishmania* parasites is a complex issue and its study is vital for the conception of possible ways to block it. To dissect the relevance of *Li*mFRD and *Li*NDH2 in *L. infantum* metabolism, mutant parasites in either *Li*mFRD (three copies in the genome) or *Li*NDH2 (two copies in the genome) encoding genes are required. To obtain the knockout mutants, the respective ORF is replaced by a gene that confers resistance to a drug. However, sometimes knockout mutants are not viable, indicating that the gene may be essential, and deletion of all the gene copies is only possible upon episomal expression of the protein.

Another important aspect that deserves further investigation is the exact localization of *Li*NDH2 protein, either facing the mitochondrial matrix or the intermembrane space. This issue is of utmost importance as it will define *Li*NDH2 as the alternative to complex I (internal enzyme) or as an enzyme that oxidizes cytosolic NADH, and thus cannot complement for the absence of complex I. To address this question, we will investigate the ability of *Li*NDH2 to complement the phenotypes of ndi1 or the double mutant nde1/nde2 of *S. cerevisiae*.

The thorough characterization of the respiratory chain of *L. infantum* amastigotes will also be pursued and compared to the promastigotes pathway. Moreover, it will be important to elucidate the effect of SHAM and KCN in promastigotes growth, namely to investigate the induction of a putative alternative oxidase.

Bibliography

1. Santos ALS, Branquinha MH, d'Avila-Levy CM, Kneipp LF, & Sodré CL (2014) Proteins and Proteomics of Leishmania and Trypanosoma. HARRIS, J R ed. Springer Dordrecht Heidelberg New York London
2. Kedzierski L, Zhu Y, & Handman E (2006) Leishmania vaccines: progress and problems. Parasitol **133 Suppl**, S87-112
3. McConville MJ & Naderer T (2011) Metabolic pathways required for the intracellular survival of Leishmania. Annu Rev Microbiol **65**, 543-561
4. Chen M, Zhai L, Christensen SB, Theander TG, & Kharazmi A (2001) Inhibition of fumarate reductase in Leishmania major and L. donovani by chalcones. Antimicrob Agents Chemother **45**, 2023-2029
5. Elmahallawy EK*, et al.* (2014) Activity of melatonin against Leishmania infantum promastigotes by mitochondrial dependent pathway. Chem Biol interact **220C**, 84-93
6. Saunders, E. C., Ng, W. W., Chambers, J. M., Ng, M., Naderer, T., Kromer, J. O., Likic, V. A., and McConville, M. J. (2011) J Biol Chem **286**, 27706-27717
7. Schurig-Briccio LA, Yano T, Rubin H, & Gennis RB (2014) Characterization of the type 2 NADH:menaquinone oxidoreductases from Staphylococcus aureus and the bactericidal action of phenothiazines. Biochim Biophys Acta **1837**, 954-963
8. Duncan R*, et al.* (2011) Identification and characterization of genes involved in leishmania pathogenesis: the potential for drug target selection. Mol Biol Int **2011**, 428486
9. Kaye P & Scott P (2011) Leishmaniasis: complexity at the host-pathogen interface. Nat Rev Microbiol **9**, 604-615
10. Gluenz E, Ginger ML, & McKean PG (2010) Flagellum assembly and function during the Leishmania life cycle. Curr Opin Microbiol **13**, 473-479
11. Opperdoes FR & Coombs GH (2007) Metabolism of Leishmania: proven and predicted. Trends Parasitol **23**, 149-158
12. Naderer T & McConville MJ (2008) The Leishmania-macrophage interaction: a metabolic perspective. Cell Microbiol **10**, 301-308
13. Saunders EC*, et al.* (2014) Induction of a stringent metabolic response in intracellular stages of Leishmania mexicana leads to increased dependence on mitochondrial metabolism. PLoS pathogens **10**, e1003888
14. Mondal S, Roy JJ, & Bera T (2014) Characterization of mitochondrial bioenergetic functions between two forms of Leishmania donovani - a comparative analysis. J Bioenerg Biomembr **46**, 395-402

15. Lodge R & Descoteaux A (2005) Modulation of phagolysosome biogenesis by the lipophosphoglycan of Leishmania. Clin Immunol **114**, 256-265
16. Heikal A*, et al.* (2014) Structure of the bacterial type II NADH dehydrogenase: a monotopic membrane protein with an essential role in energy generation. Mol Microbiol **91**, 950-964
17. Saunders EC*, et al.* (2010) Central carbon metabolism of Leishmania parasites. Parasitol **137**, 1303-1313
18. Bringaud F, Riviere L, & Coustou V (2006) Energy metabolism of trypanosomatids: adaptation to available carbon sources. Mol Biochem Parasitol **149**, 1-9
19. Tielens AG & van Hellemond JJ (2009) Surprising variety in energy metabolism within Trypanosomatidae. Trends Parasitol **25**, 482-490
20. Rosenzweig D*, et al.* (2008) Retooling Leishmania metabolism: from sand fly gut to human macrophage. FASEB J **22**, 590-602
21. Rainey PM & MacKenzie NE (1991) A carbon-13 nuclear magnetic resonance analysis of the products of glucose metabolism in Leishmania pifanoi amastigotes and promastigotes. Mol Biochem Parasitol **45**, 307-315
22. Coustou V*, et al.* (2005) A mitochondrial NADH-dependent fumarate reductase involved in the production of succinate excreted by procyclic Trypanosoma brucei. J Biol Chem **280**, 16559-16570
23. Van Weelden SW, van Hellemond JJ, Opperdoes FR, & Tielens AG (2005) New functions for parts of the Krebs cycle in procyclic Trypanosoma brucei, a cycle not operating as a cycle. J Biol Chem **280**, 12451-12460
24. Naderer T*, et al.* (2006) Virulence of Leishmania major in macrophages and mice requires the gluconeogenic enzyme fructose-1,6-bisphosphatase. Proc Natl Acad Sci USA **103**, 5502-5507
25. Ginger ML, Fairlamb AH, & Opperdoes FR (2007) Comparative genomics of trypanosome metabolism. In Trypanosomes: after the genome. Horizon Bioscience, London, 373-417
26. Ebikeme C*, et al.* (2010) Ablation of succinate production from glucose metabolism in the procyclic trypanosomes induces metabolic switches to the glycerol 3-phosphate/dihydroxyacetone phosphate shuttle and to proline metabolism. J Biol Chem **285**, 32312-32324
27. Verner Z*, et al.* (2011) Complex I (NADH:ubiquinone oxidoreductase) is active in but non-essential for procyclic Trypanosoma brucei. Mol Biochem Parasitol **175**, 196-200

28. Shaked-Mishan P*, et al.* (2006) A novel high-affinity arginine transporter from the human parasitic protozoan Leishmania donovani. Mol Microbiol **60**, 30-38
29. Akerman M, Shaked-Mishan P, Mazareb S, Volpin H, & Zilberstein D (2004) Novel motifs in amino acid permease genes from Leishmania. Biochem Biophys Res Commun **325**, 353-366
30. Tomas AM & Castro H (2013) Redox metabolism in mitochondria of trypanosomatids. Antioxid Redox Signal **19**, 696-707
31. Menna-Barreto RF & de Castro SL (2014) The double-edged sword in pathogenic trypanosomatids: the pivotal role of mitochondria in oxidative stress and bioenergetics. BioMed Res Int **2014**, 614014
32. Turrens JF (2012) The Enzyme NADH-fumarate Reductase in Trypanosomatids: a potential Target against Parasitic Diseases. Mol Cell Pharm **4(3)**, 117-122
33. Dey R*, et al.* (2010) Characterization of a Leishmania stage-specific mitochondrial membrane protein that enhances the activity of cytochrome c oxidase and its role in virulence. Mol Microbiol **77**, 399-414
34. Feng Y*, et al.* (2012) Structural insight into the type-II mitochondrial NADH dehydrogenases. Nature **491**, 478-482
35. Verner Z*, et al.* (2014) Comparative analysis of respiratory chain and oxidative phosphorylation in Leishmania tarentolae, Crithidia fasciculata, Phytomonas serpens and procyclic stage of Trypanosoma brucei. Mol Biochem Parasitol **193**, 55-65
36. Voulgaris I, O'Donnell A, Harvey LM, & McNeil B (2012) Inactivating alternative NADH dehydrogenases: enhancing fungal bioprocesses by improving growth and biomass yield? Sci Rep **2**, 322
37. Opperdoes FR & Michels PA (2008) Complex I of Trypanosomatidae: does it exist? Trends Parasitol **24**, 310-317
38. Chaudhuri M, Ott RD, & Hill GC (2006) Trypanosome alternative oxidase: from molecule to function. Trends Parasitol **22**, 484-491
39. Van Hellemond JJ & Tielens AG (1997) Inhibition of the respiratory chain results in a reversible metabolic arrest in Leishmania promastigotes. Mol Biochem Parasitol **85**, 135-138
40. Hernandez FR & Turrens JF (1998) Rotenone at high concentrations inhibits NADH-fumarate reductase and the mitochondrial respiratory chain of Trypanosoma brucei and T. cruzi. Mol Biochem Parasitol **93**, 135-137

41. Duarte M & Tomas AM (2014) The mitochondrial complex I of trypanosomatids - an overview of current knowledge. J Bioenerg Biomembr **46**, 299-311
42. Kerscher SJ, Okun JG, & Brandt U (1999) A single external enzyme confers alternative NADH:ubiquinone oxidoreductase activity in Yarrowia lipolytica. J Cell Sci **112**, 2347-2354
43. Fang J & Beattie DS (2002) Novel FMN-containing rotenone-insensitive NADH dehydrogenase from Trypanosoma brucei mitochondria: isolation and characterization. Biochemistry **41**, 3065-3072
44. Melo AM, Bandeiras TM, & Teixeira M (2004) New insights into type II NAD(P)H:quinone oxidoreductases. Microbiol Mol Biol Rev **68**, 603-616
45. Iwata M*, et al.* (2012) The structure of the yeast NADH dehydrogenase (Ndi1) reveals overlapping binding sites for water- and lipid-soluble substrates. Proc Natl Acad Sci USA **109**, 15247-15252
46. Matus-Ortega MG*, et al.* (2011) The alternative NADH dehydrogenase is present in mitochondria of some animal taxa. Comparative biochemistry and physiology. Part D, Genomics & Kerscher SJ (2000) Biochim Biophys Acta **1459**, 274-283
47. Kerscher SJ (2000) Diversity and origin of alternative NADH:ubiquinone oxidoreductases. Biochim Biophys Acta **1459**, 274-283
48. Soole KL & Menz RI (1995) Functional molecular aspects of the NADH dehydrogenases of plant mitochondria. J Bioenerg Biomembr **27**, 397-406
49. Teh JS, Yano T, & Rubin H (2007) Type II NADH: menaquinone oxidoreductase of Mycobacterium tuberculosis. Infect Disord Drug Targets **7**, 169-181
50. Duarte M, Peters M, Schulte U, & Videira A (2003) The internal alternative NADH dehydrogenase of Neurospora crassa mitochondria. Biochem J **371**, 1005-1011
51. Carneiro P, Duarte M, & Videira A (2004) The main external alternative NAD(P)H dehydrogenase of Neurospora crassa mitochondria. Biochim Biophys Acta **1608**, 45-52
52. Gonzalez-Halphen D & Maslov DA (2004) NADH-ubiquinone oxidoreductase activity in the kinetoplasts of the plant trypanosomatid Phytomonas serpens. Parasitol Res **92**, 341-346
53. Rasmusson AG, Svensson AS, Knoop V, Grohmann L, & Brennicke A (1999) Homologues of yeast and bacterial rotenone-insensitive NADH dehydrogenases in higher eukaryotes: two enzymes are present in potato mitochondria. Plant J **20**, 79-87

54. De Vries S, Van Witzenburg R, Grivell LA, & Marres CA (1992) Primary structure and import pathway of the rotenone-insensitive NADH-ubiquinone oxidoreductase of mitochondria from Saccharomyces cerevisiae. Eur J Biochem **203**, 587-592
55. Marres CA, de Vries S, & Grivell LA (1991) Isolation and inactivation of the nuclear gene encoding the rotenone-insensitive internal NADH: ubiquinone oxidoreductase of mitochondria from Saccharomyces cerevisiae. Eur J Biochem **195**, 857-862
56. Small WC & McAlister-Henn L (1998) Identification of a cytosolically directed NADH dehydrogenase in mitochondria of Saccharomyces cerevisiae. J Bacteriol **180**, 4051-4055
57. Kerscher S, Drose S, Zwicker K, Zickermann V, & Brandt U (2002) Yarrowia lipolytica, a yeast genetic system to study mitochondrial complex I. Biochim Biophys Acta **1555**, 83-91
58. Dong CK*, et al.* (2009) Type II NADH dehydrogenase of the respiratory chain of Plasmodium falciparum and its inhibitors. Bioorg Med Chem lett **19**, 972-975
59. Lin SS, Gross U, & Bohne W (2011) Two internal type II NADH dehydrogenases of Toxoplasma gondii are both required for optimal tachyzoite growth. Mol Microbiol **82**, 209-221
60. Fang J & Beattie DS (2003) Identification of a gene encoding a 54 kDa alternative NADH dehydrogenase in Trypanosoma brucei. Mol Biochem Parasitol **127**, 73-77
61. Verner Z*, et al.* (2013) Alternative NADH dehydrogenase (NDH2): intermembrane-space-facing counterpart of mitochondrial complex I in the procyclic Trypanosoma brucei. Parasitol **140**, 328-337
62. Christmas PB & Turrens JF (2000) Separation of NADH-fumarate reductase and succinate dehydrogenase activities in Trypanosoma cruzi. FEMS Microbiol Lett **183**, 225-228
63. Merlino A, Vieites M, Gambino D, & Coitino EL (2014) Homology modeling of T. cruzi and L. major NADH-dependent fumarate reductases: ligand docking, molecular dynamics validation, and insights on their binding modes. J Mol Graph Model **48**, 47-59
64. Castro H*, et al.* (2004) Two linked genes of Leishmania infantum encode tryparedoxins localised to cytosol and mitochondrion. Mol Biochem Parasitol **136**, 137-147

65. Sousa AF*, et al.* (2014) Genetic and chemical analyses reveal that trypanothione synthetase but not glutathionylspermidine synthetase is essential for Leishmania infantum. Free Radic Biol Med **73**, 229-238
66. Roberts SC*, et al.* (2004) Arginase plays a pivotal role in polyamine precursor metabolism in Leishmania. Characterization of gene deletion mutants. J Biol Chem **279**, 23668-23678
67. Melo AM*, et al.* (2001) The external calcium-dependent NADPH dehydrogenase from Neurospora crassa mitochondria. J Biol Chem **276**, 3947-3951
68. Skodova I*, et al.* (2013) Characterization of two mitochondrial flavin adenine dinucleotide-dependent glycerol-3-phosphate dehydrogenases in Trypanosoma brucei. Eukaryot Cell **12**, 1664-1673
69. Pahlman IL*, et al.* (2002) Kinetic regulation of the mitochondrial glycerol-3-phosphate dehydrogenase by the external NADH dehydrogenase in Saccharomyces cerevisiae. J Biol Chem **277**, 27991-27995
70. Bunoust O, Devin A, Averet N, Camougrand N, & Rigoulet M (2005) Competition of electrons to enter the respiratory chain: a new regulatory mechanism of oxidative metabolism in Saccharomyces cerevisiae. J Biol Chem **280**, 3407-3413
71. Coustou V*, et al.* (2008) Glucose-induced remodeling of intermediary and energy metabolism in procyclic Trypanosoma brucei. J Biol Chem **283**, 16342-16354
72. Niemann M*, et al.* (2013) Mitochondrial outer membrane proteome of Trypanosoma brucei reveals novel factors required to maintain mitochondrial morphology. Mol Cell Proteomics **12**, 515-528
73. Maldonado EN & Lemasters JJ (2014) ATP/ADP ratio, the missed connection between mitochondria and the Warburg effect. Mitochondrion, doi: 10.1016/j.mito.2014.09.002.

Supplementary

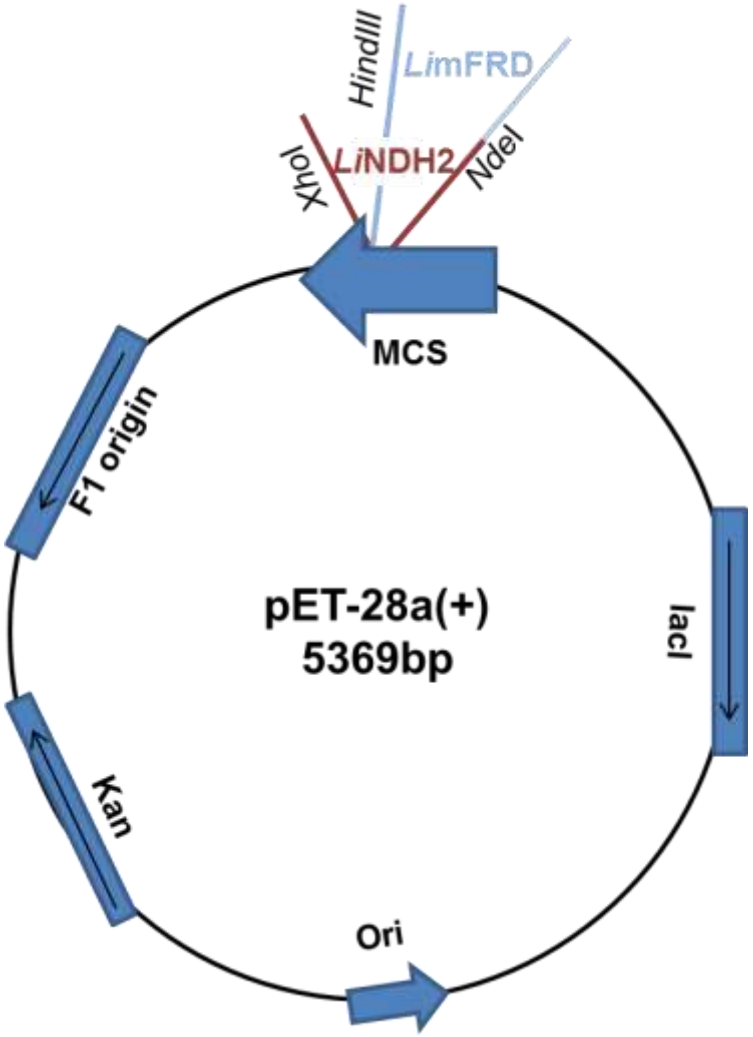

Figure 25. Representation of the expression plasmids pET28_6His*Li*mFRD and pET28_6His*Li*NDH2. This vector was used for expression of *L.infantum* mitochondrial fumarate reductase and alternative NADH dehydrogenase.

Table 8. Values used for determination of the oxygen consumption rates of the indicated strains. The numbers in red were excluded from the analysis.

	nmol O_2.min^{-1}.mg^{-1}								
	Basal oxygen consumption			**+ TTFA**			**+ TTFA+KCN**		
	WT	**OE_*Li*mFRD-cMyc**	**OE_*Li*NDH2-cMyc**	**WT**	**OE_*Li*mFRD-cMyc**	**OE_*Li*NDH2-cMyc**	**WT**	**OE_*Li*mFRD-cMyc**	**OE_*Li*NDH2-cMyc**
	26.20	22.72	25.94				0.40	1.92	1.85
	15.04	14.40	21.31		9.39	11.23		5.55	3.14
	20.85	17.68	27.33	5.81	6.23	6.79	0.85	2.51	0.72
	18.09	22.57	18.75	5.90	10.74		0.66	4.71	
	15.1	10.27	19.19		7.83	4.97		5.23	0.04
	10.85	12.42	23.66	2.60	6.61	9.61		5.38	1.52
	19.13	13.91	22.63	10.20	6.43	13.03	3.33	3.65	4.57
	19.21	10.30	18.99	8.58			1.80		
	20.00			10.42					
	11.25			5.42			2.25		
	11.70								
	12.50								
Average	16.66	15.53	22.23	6.99	7.87	9.13	1.55	4.14	1.97
SD	4.71	4.99	3.27	2.86	1.84	3.26	1.12	1.46	1.65